

Tectonic and magmatic evolution of the mantle lithosphere during the rifting stages of a fossil slow–ultraslow spreading basin: insights from the Erro–Tobbio peridotite (Voltri Massif, NW Italy)

MATTEO PADOVANO¹*, GIOVANNI B. PICCARDO² & REINOUD L. M. VISSERS³

¹*Via XXV Aprile 37, 16012, Bargagli, Genova, Italy*

²*Via Sturla 33/4, 16131 Genova, Italy*

³*Department of Earth Sciences, Utrecht University, PO Box 80021, 3508TA Utrecht, The Netherlands*

**Corresponding author (e-mail: matte.pado@hotmail.it)*

Abstract: We investigate the structural, petrological and compositional features recorded by strongly deformed and melt-percolated Erro–Tobbio peridotites (Voltri Massif, Ligurian Alps, NW Italy), in order to demonstrate that the processes of shear-zone formation and melt percolation are intimately linked by a positive feedback. We focus on spinel and plagioclase peridotites, and extensional shear zones that underwent infiltration by upwelling asthenospheric melts. Shear and porosity bands, which developed during extension prior to melt infiltration, represent important structural and rheological pathways to facilitate and enhance melt infiltration into the extending lithosphere and the ascent of such melts to shallower levels.

Our results lend strong support to numerical models addressing the physical processes underlying extensional systems. These show that, in the case of slow–ultraslow continental extension and the subsequent formation of slow–ultraslow spreading oceans, porosity and shear-localization bands may develop in a previously unstructured lithosphere, prior to melt infiltration. Our studies on the Erro–Tobbio peridotites allow a model for the inception of continental extension and rifting to drifting of slow–ultraslow spreading oceans to be proposed. We suggest that integrated studies of on-land peridotites, coupled with geophysical–structural results from modern oceans, may provide clues to the geodynamic processes governing continental extension and passive rifting.

The Voltri Massif (Ligurian Alps, NW Italy) is the largest ophiolite massif of the Western Alpine–Northern Apennine chain (Fig. 1), and is a remnant of the Jurassic Ligurian Tethys.

The Erro–Tobbio peridotites represent a portion of the Insubrian (Adria) subcontinental mantle that was first exhumed during the lithosphere extension and rifting of the Jurassic Ligurian Tethys Basin, and exposed at the Adriatic ocean–continent transition (OCT). It was subsequently subjected to high-pressure eclogite-facies conditions during basin closure, followed by exhumation in an antigorite-dominated subduction channel (Piccardo 2012 and references therein). Despite the Alpine overprint, large domains of Erro–Tobbio peridotite have preserved mantle textures and mineral assemblages that allow studies of their pre-Alpine mantle evolution to be undertaken. Previous structural studies (e.g. Drury *et al.* 1990; Hoogerduijn Strating *et al.* 1990, 1993; Vissers *et al.* 1991) of the rifting evolution of the Erro–Tobbio mantle rocks inferred that, in response to lithospheric extension, the Erro–Tobbio peridotites were exhumed along a

subsidiary pressure–temperature (P – T) trajectory, starting from subcontinental lithospheric mantle depths ($T < 1000$ – 1100 °C and spinel-facies conditions) and accommodated by five generations of km-scale extensional shear zones active under decreasing P – T conditions (spinel-bearing tectonites, plagioclase-, hornblende- and chlorite-bearing peridotite mylonites, and serpentine mylonites). The occurrence, in the spinel peridotites, of orthopyroxene + spinel clusters, which were interpreted as breakdown products of pre-existing mantle garnets (Hoogerduijn Strating *et al.* 1993), prompted the suggestion that pristine mantle peridotites underwent spinel-facies equilibration after upwelling from garnet-facies conditions.

Geochemical investigations on depleted spinel peridotites revealed that the bulk-rock and mineral chemistry show chemical contrasts indicating that these peridotites were affected by melt–peridotite interaction during reactive porous melt flow (Rampone *et al.* 2004). Piccardo & Vissers (2007) provided evidence that the subsolidus evolution recorded by the Erro–Tobbio peridotites was

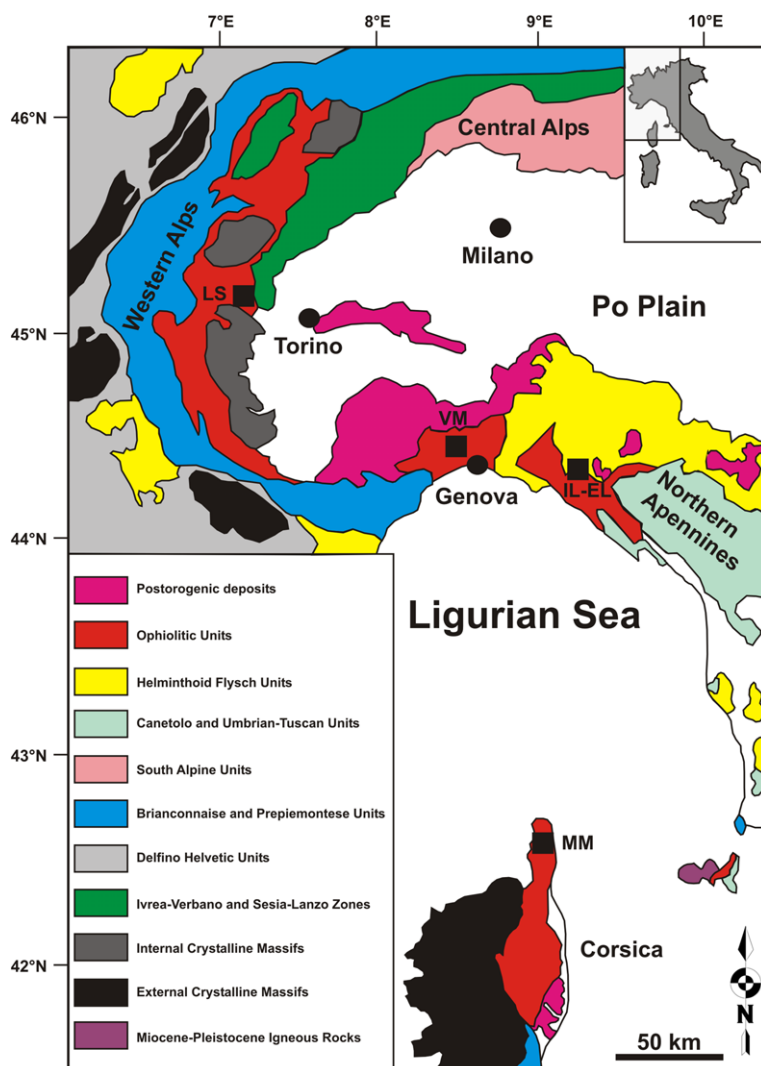


Fig. 1 Location of the main ophiolitic massifs pertaining to the Jurassic Ligurian Tethys. LS, South Lanzo; VM, Voltri Massif; IL, Internal Ligurides; EL, External Ligurides; MM, Monte Maggiore–Corsica. Redrawn and modified after Piccardo *et al.* (2014) and Piccardo (2014 and references therein).

accompanied by a diffuse melt-related evolution, characterized by the migration through the extending mantle lithosphere of mid-ocean ridge basalt (MORB)-type melts formed by decompression melting of the underlying asthenosphere during near-adiabatic upwelling. On the basis of their structural and compositional features, Piccardo & Vissers (2007) distinguished four different rock types:

- *Lithospheric spinel peridotites*: the oldest rock type that preserves relicts of metamorphic reactions, and bulk-rock and mineral compositions indicating refractory residual characteristics and

a stage of high-pressure–high-temperature equilibration in the mantle lithosphere.

- *Reactive spinel peridotites*: pyroxene-depleted harzburgitic rocks that show microstructures reflecting melt–peridotite reactions, and bulk-rock, modal and mineral compositions that are significantly modified due to reactions with percolating pyroxene(-silica)-undersaturated melts compared with the lithospheric peridotites.
- *Impregnated plagioclase peridotites*: plagioclase-enriched peridotites that show melt–peridotite reaction microstructures, and are enriched in microgranular gabbro-noritic aggregates formed

by the interstitial crystallization of percolating orthopyroxene(-silica)-saturated melts.

- *Replacive spinel dunites*: almost pyroxene-free granular rocks formed by the focused reactive percolation of pyroxene-undersaturated melts along compositional or structural discontinuities, leading to complete pyroxene dissolution of the precursor peridotites.

The above studies elucidated the structural and petrological processes recorded by the Erro–Tobbio ultramafics during their pre-Alpine history, and emphasized the role of melt percolation and stagnation into the extended lithosphere. However, the mutual relationships between progressive shear-zone formation and percolation of asthenospheric melts have never been thoroughly investigated. In this paper we address the structural, petrological and compositional features recorded by strongly deformed and melt-percolated Erro–Tobbio peridotites in order to demonstrate that the processes of shear-zone formation and melt percolation are intimately linked by a positive feedback. In particular, we show that the migration of asthenospheric melts within the lithospheric mantle was favoured by the development of translithospheric extensional shear zones and that the presence of high-temperature melts within these shear zones enhanced further strain accumulation. This leads us to discuss with more accuracy the effects of weakening and thermo-chemical-mechanical erosion of the lithosphere, previously envisaged by Piccardo (2003), and investigated by Corti *et al.* (2007) and Ranalli *et al.* (2007). These are the main factors considered responsible for the rapid transition from continental extension and rifting to whole-lithosphere failure and seafloor spreading.

State of the art on rifting and opening of the Jurassic Ligurian Tethys

Rifting stage

The Ligurian Tethys Basin separated Europe and Adria in Late Jurassic–Cretaceous times. Its opening was kinematically related to pre-Jurassic rifting and Late Jurassic spreading in the central Atlantic, and was presumably a consequence of the passive stretching of the Europe–Adria continental lithosphere by far-field tectonic forces (Piccardo *et al.* 2009; Vissers *et al.* 2013). Extension in the Europe–Adria system was already active during Triassic times, as constrained by geochronological data inferred from extensional shear zones within the External Ligurides peridotites (220 ± 13 Ma, Lu–Hf isochrons on pyroxenites: Montanini *et al.* 2006) and from the Malenco peridotites

(225 Ma, $^{40}\text{Ar}/^{39}\text{Ar}$ ages on amphiboles: Müntener & Hermann 2001).

On the basis of stratigraphic and sedimentological evidence, Whitmarsh & Manatschal (2012) suggested that during the Upper Triassic–Lower Jurassic (c. 200 Ma) rifting was first distributed over the whole margin, leading to subsidence and formation of fault-bounded half-graben in the proximal parts of the margin. This notion is corroborated by Capitanio & Goes (2006), who proposed that the onset of major rifting occurred in Liassic times (c. 190 Ma; see also Vissers *et al.* 2013). Lithospheric extension and stretching facilitated the progressive passive adiabatic upwelling of the asthenosphere, which underwent partial melting under decompression and produced the early percolation of melts within the extended mantle lithosphere (Piccardo *et al.* 2004b, c, 2009; Piccardo 2008, 2010; Piccardo & Guarnieri 2011; Guarnieri *et al.* 2012).

Rift-related magmatism

Recent studies have shown that in their evolution from rifting to spreading, two main magmatic events are recorded by the Ligurian Tethys ophiolites: the early ‘hidden’ magmatism and the late ‘oceanic’ magmatism (see Piccardo *et al.* 2014 and references therein). The early ‘hidden’ magmatism is represented by early asthenospheric single fractional melt increments that migrated through the rifted mantle lithosphere via diffuse or focused porous flow, and induced melt–peridotite interaction and interstitial melt crystallization, sometimes forming small intrusive gabbro–norite bodies. These melts stagnated and were stored in the shallow-mantle lithosphere, under plagioclase-peridotite-facies conditions; they never reached the seafloor because lavas with their composition have never been found within oceanic volcanic rocks. One sample of a gabbro–norite vein from Monte Maggiore (Corsica) yielded whole-rock–clinopyroxene–plagioclase (WR–cpx–plg) Sm–Nd isochron ages of 155 ± 6 Ma (Rampone *et al.* 2009). The age of the hidden magmatism is as yet not sufficiently constrained, but it most probably occurred in Middle Jurassic times. The late ‘oceanic’ magmatism is represented by normal-MORB (N-MORB) melts which migrated within high-porosity dunite channels and reached shallow lithospheric levels, where they intruded into the shallow mantle as olivine-gabbro bodies and related rocks, and extruded at the seafloor as basaltic lavas (Piccardo *et al.* 2014 and references therein). According to Rampone & Piccardo (2000 and references therein), olivine gabbros from the Internal Liguride ophiolites define a Sm–Nd mineral isochron age of 164 ± 14 Ma. Olivine-gabbro samples from Monte Maggiore (Corsica) yielded WR–cpx–plg Sm–Nd isochron

ages of 162 ± 10 and 159 ± 15 Ma (Rampone *et al.* 2009). On the basis on new and literature U–Pb data, Li *et al.* (2013 and references therein) have recently defined a nearly synchronous time interval of crystallization at 166–158 Ma for all the ophiolitic olivine gabbros and differentiates from the Eastern, Central and Western Alps, Liguria and Corsica.

Spreading stage

According to Vissers *et al.* (2013), the Jurassic–Early Cretaceous motions of Africa–Meseta and Iberia with respect to North America allow the kinematics of extension and spreading in the Ligurian Tethys east of Iberia to be estimated (Fig. 2). They interpreted the Adria path as the expression of some 450 km of extension, largely between 170 and about 148 Ma, during which oceanic spreading may have occurred in the western Ligurian Tethys. The time-averaged, slow to very slow, full spreading rate is estimated to be 22.7 mm a^{-1} , in line with the onset of spreading between Iberia and North America. Vissers *et al.* (2013) addressed the evolution of the Ligurian Tethys further to the east, where Africa–Europe rather than Africa–Iberia motion determined its opening. The Alpine Tethys continued eastwards along the length of the Alps, where Adria and its NE intensely deformed promontory became separated from Eurasia. This was accommodated by the opening of the Valais Basin and the Piemonte Ocean, which were separated by the Briançonnais microcontinental sliver (e.g. Frisch 1979; Schmid *et al.* 2004). To the west, in the domain of the present-day Western

Alps, Africa–Europe extension was at best around 675 km, part of which was accommodated in the Valais Basin (e.g. Schmid *et al.* 2004). Although the partitioning of the extension between the Valais and Ligurian–Piedmontese domains is difficult to assess, it can be inferred from these values that the spreading rates across the entire Ligurian Tethys were slow–ultraslow. This kinematic analysis confirms the results of several studies suggesting that the Ligurian Tethys was comparable to modern slow-spreading oceans, such as the Atlantic (Lemoine *et al.* 1987; Lagabrielle & Cannat 1990; Cannat 1996; Cannat *et al.* 1997; Lagabrielle & Lemoine 1997; Magde *et al.* 2000; Rabain *et al.* 2001). Moreover, the slow–ultraslow nature of the Ligurian Tethys has been inferred by stratigraphic, structural and petrological studies on Alpine and Apenninic ophiolites (e.g. Tribuzio *et al.* 2000; Piccardo 2008, 2010).

The Voltri Massif

The Voltri Massif is the largest metamorphic ophiolite Massif in the Alpine–Apennine chain. It is located in the easternmost part of the Ligurian Alps (northern Italy), and is separated from the Ligurian Northern Apennines to the east by the Sestri–Vtaggio zone (see Piccardo 2012, 2013 and references therein). The Voltri Massif is composed of: (1) calc-schists (metamorphic oceanic sediments); (2) prasinites (metamorphic MORB-type oceanic volcanics); (3) high-pressure meta-gabbros, eclogites and rodingites (metamorphic MORB-type oceanic intrusives); and (4) huge masses of variably serpentinized mantle peridotites

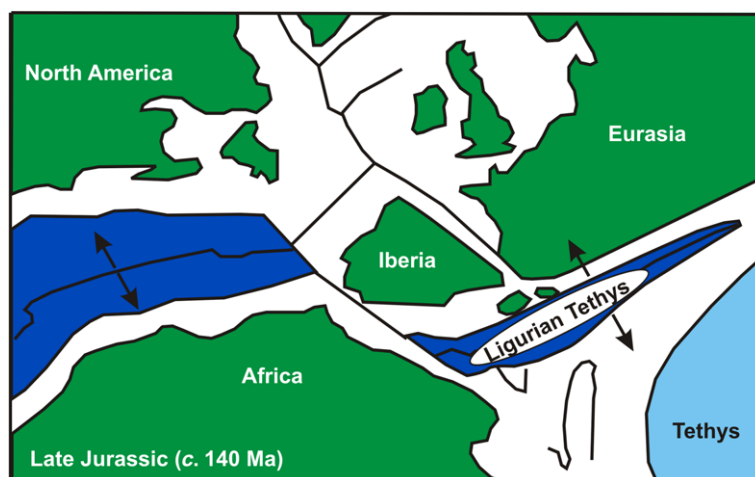


Fig. 2. Plates and plate motions involved in the opening of the Ligurian Tethys Ocean. Palaeogeography pertains to the Late Jurassic (c. 140 Ma). Redrawn and modified after Vissers *et al.* (2013), adapted from Frisch (1979).

and antigorite serpentinites (e.g. Messiga & Piccardo 1974).

Chiesa *et al.* (1975) recognized different structural units, among which are: (1) the Voltri–Rossiglione Unit, consisting of calc-schists and prasinites (i.e. MORB meta-volcanic rocks), showing relicts of high-pressure assemblages; (2) the Beigua Unit, consisting of antigorite serpentinites with relicts of high-pressure assemblages (metamorphic, Mn-rich-olivine-bearing antigorite schists) and eclogitic–rodingitic meta-gabbros; and (3) the Erro–Tobbio Unit, consisting of almost unaltered to variably serpentinized mantle peridotites. They suggested that the oceanic lithosphere of the Europe plate underwent eastward subduction under the Insubrian (Adria) margin, and that the tectonic units of the Voltri Massif were tectonically exhumed and emplaced onto the Briançonnaise (Europe) margin. They believed that the Erro–Tobbio peridotites were derived from the Insubrian (Adria) subcontinental lithosphere and thrust above the high-pressure units of the Voltri Massif during continental collision, without having undergone subduction. Accordingly, the Voltri Massif was considered a nappe stack formed by peridotites, antigorite serpentinites and metamorphic oceanic sediments, piled westwards onto the European margin during closure of the Ligurian Tethys (Chiesa *et al.* 1975).

From the middle of the 1970s, the presence of Mn-rich-olivine + antigorite (\pm Ti-clinohumite \pm diopside \pm chlorite) mineral assemblages was described in the Voltri Massif antigorite serpentinites and it was recognized that they recrystallized at the highest P – T conditions reached during subduction, comparable to the eclogitic recrystallization of the mafic rocks (see references in Piccardo 2012, 2013). At the end of the 1980s, the presence of olivine + antigorite + Ti-clinohumite assemblages in the Erro–Tobbio peridotites, partly replacing mantle minerals, indicated that these peridotites also underwent subduction to high-pressure (eclogitic) conditions (Piccardo *et al.* 1989; Scambelluri *et al.* 1991).

Since the work of Chiesa *et al.* (1975), the Beigua antigorite serpentinites, which are associated in the field with metamorphic ophicalcites and pillow-breccias and metamorphic oceanic volcanic–sedimentary cover (i.e. calc-schists and meta-volcanics), were included within the oceanic lithosphere of the Ligure–Piedmontese (Ligurian Tethys) Basin, whereas the Erro–Tobbio peridotites were related to the Insubrian (Adria) subcontinental mantle (e.g. Piccardo *et al.* 1977; Drury *et al.* 1990; Piccardo & Vissers 2007; and references therein). The Beigua unit is thus thought to represent subducted and dismembered oceanic lithosphere of the Ligurian Tethys, whereas the Erro–Tobbio peridotites are interpreted as subcontinental mantle

from the Adria margin (i.e. the hanging wall of the subduction zone: see more information in Piccardo 2012, 2013).

In summary, the Ligurian Tethys was formed by continental extension within the Europe–Adria lithosphere and eventually consisted of seafloor-exposed mantle peridotites with an uppermost layer of oceanic serpentinites and widespread oceanic sediments and MORB volcanics, and of subcontinental lithospheric mantle exhumed at the Adria extended continental margins (OCT). Plate convergence caused eastward subduction of the oceanic lithosphere of the Europe plate.

Regarding the Voltri Massif, it has been proposed that the uppermost serpentinite layer of the subducting slab formed a serpentinite-subduction channel (see Malatesta *et al.* 2011, 2012a, b; Piccardo 2012, 2013; and references therein). Sectors of the mantle lithosphere of the Adria extended margin (the future Erro–Tobbio peridotites) underwent ablative subduction, and were detached, embedded and buried to eclogite-facies conditions within the serpentinite-subduction channel (Piccardo 2012, 2013). The serpentinite-subduction channel (future Beigua serpentinites), acting as a low-viscosity carrier for high-density subducted rocks, should have played a fundamental role in the exhumation dynamics, allowing rapid exhumation of the included Erro–Tobbio peridotite megaboudins (i.e. of the almost unaltered Adria peridotites: future Erro–Tobbio peridotites) and their emplacement into the Voltri Massif orogenic edifice (e.g. Malatesta *et al.* 2012a, b; Piccardo 2012, 2013; and references therein). Moreover, because of numerous Alpine faults, the Erro–Tobbio peridotite blocks have been rotated, as witnessed by the strongly heterogeneous orientation of foliation planes and mineral lineations.

As a consequence of this subduction and exhumation history, the Erro–Tobbio peridotites do not form a continuous structural unit, as previously inferred by Chiesa *et al.* (1975), but consist of separate km-scale mega-boudins embedded in the Beigua antigorite serpentinite (Piccardo 2012, 2013). Owing to this structural setting, the Erro–Tobbio ultramafic bodies were only partially affected by the subduction-related Alpine deformation and recrystallization, and preserve the structural and compositional features of their polyphasic pre-Alpine tectonic evolution.

The Erro–Tobbio peridotites

Structural features of Erro–Tobbio peridotites

In the following subsections, we describe mesoscale and microstructural features that testify to mantle exhumation during pre-oceanic continental rifting:

that is, both a decompressional evolution linked to the development of extensional shear zones and the interaction with asthenospheric melts. We summarize the main structural and petrological characteristics of the four different rock types recognized by Piccardo & Vissers (2007) listed earlier: that is, lithospheric spinel peridotites; reactive spinel peridotites; impregnated plagioclase peridotites; and replacive dunites. As we want to investigate the relationships between deformation and melt percolation, we do not investigate structural and compositional features linked to the downward percolation of continental or oceanic hydrous fluids. For this reason, hornblende- and chlorite-bearing

peridotite mylonites and serpentinite mylonites (e.g. Hoogerduijn Strating *et al.* 1993) will not be discussed.

Our fieldwork has been focused on an approximately 5 km² area, comprising that region between Mt Poggio, Mt Costa Lavezzara and the Badana lake (Fig. 3). This area is characterized by the presence of large outcrops of Ero–Tobbio ultramafics embedded in a matrix mostly consisting of Beigua serpentinites.

Lithospheric spinel peridotites. The mantle *protolith*: the structurally oldest rock type, which we refer to here as the mantle protolith, shows a banded

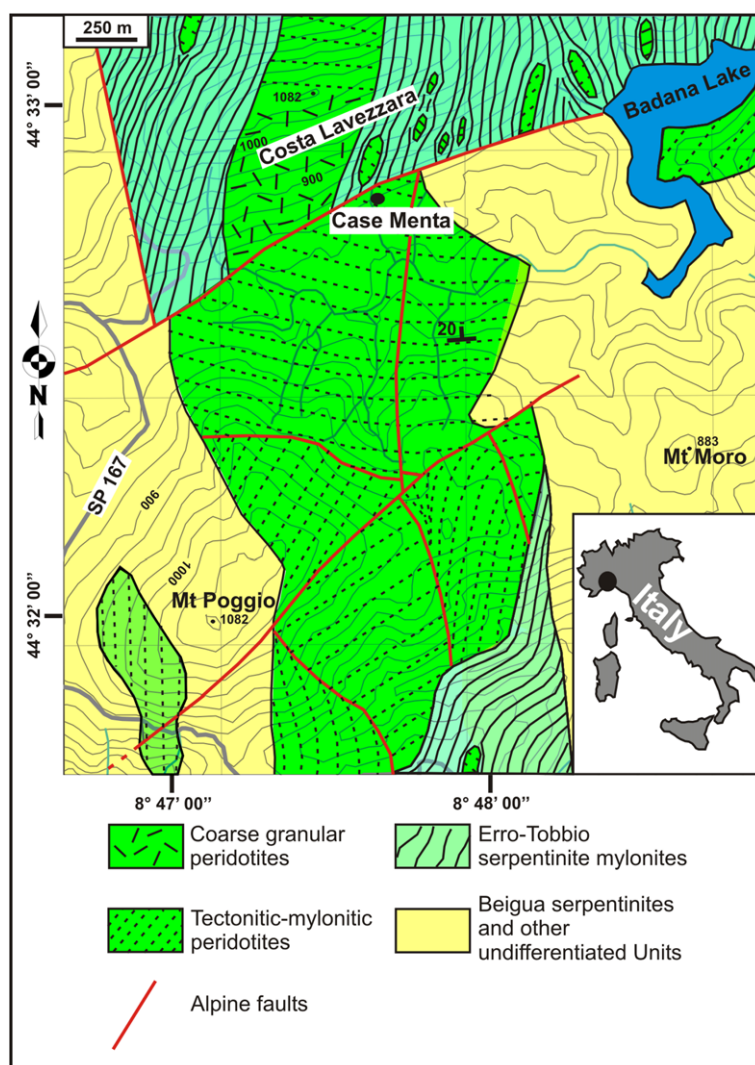


Fig. 3. Structural and tectonic sketch map of the study area.

structure marked by strongly depleted harzburgite layers alternating with clinopyroxene-rich layers. Both layers are characterized, at the macro- and microscale, by the occurrence of broadly rounded intergrowths (clusters) of orthopyroxene

(opx) + spinel (sp) (Figs 4a & 5a). The banded mantle protolith is often completely recrystallized under spinel-facies conditions, and may show a typical homogeneous and coarse-grained granular texture. The granular lherzolites preserve the opx + sp



Fig. 4. Field aspects of the Erro–Tobbio peridotites in the study area. (a) Granular lithospheric spinel-facies mantle protolith, showing abundant sp + opx clusters (spinel-facies breakdown of precursor mantle garnet); (b) isoclinal fold in spinel-facies shear zone; (c) spinel-facies tectonite–mylonite in the shear zone; (d) granular, pyroxene-depleted spinel harzburgite band inside the shear-zone tectonite; (e) granular pyroxene-depleted spinel harzburgite bands preserving relicts of iso-orientated bands in a previous spinel-facies shear zone; (f) isotropic plagioclase-enriched impregnated peridotite; (g) plagioclase-facies shear zone (vertical), cutting a previous spinel-facies shear zone at a high angle; (h) replacive spinel dunite band following the shear foliation of a plagioclase-facies shear band.

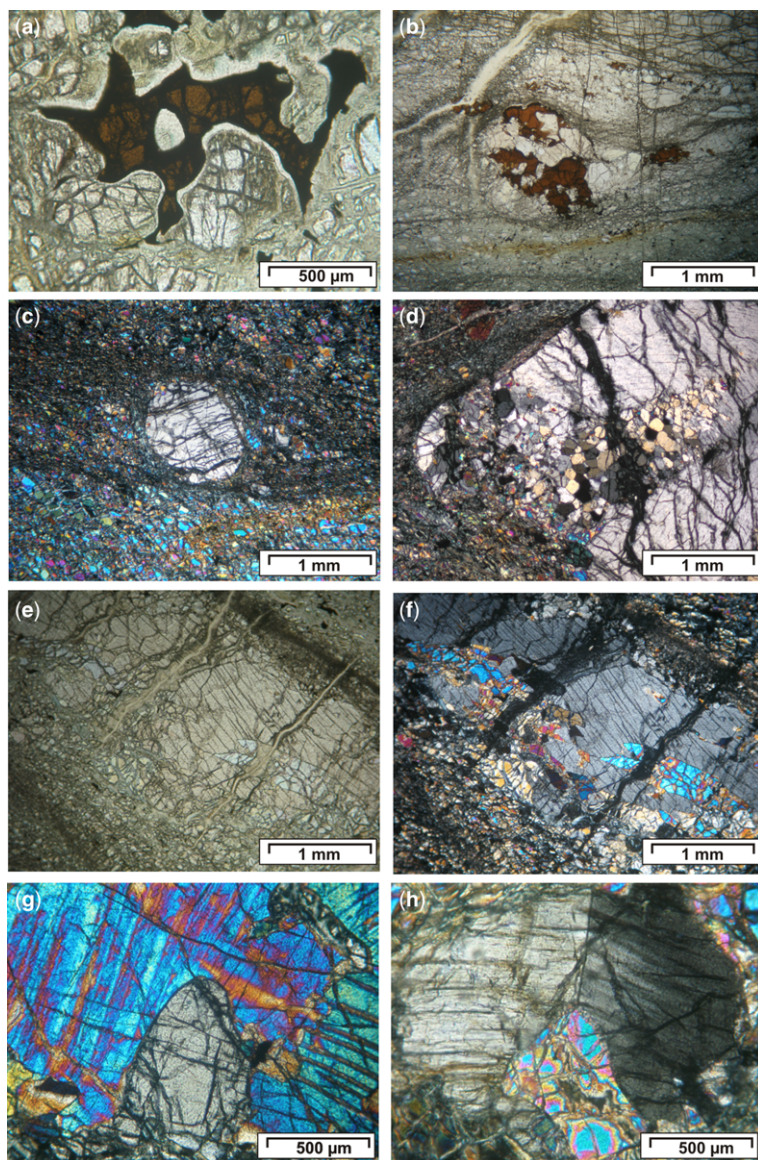


Fig. 5. Microstructures in tectonite-mylonite shear zones of the Erro-Tobbio peridotites from the study area.

(a) Spinel + orthopyroxene cluster in a granular spinel peridotite; (b) spinel + orthopyroxene cluster preserved as porphyroblast in a spinel-facies tectonite-mylonite shear zone; (c) sigmoidal rotated orthopyroxene porphyroblast in a spinel-facies tectonite-mylonite shear zone; note the grain shape fabric of olivine oblique to the main shear foliation; (d) orthopyroxene porphyroblast preserving a spinel-facies granoblastic aggregate; (e) & (f) idiomorphic undeformed blades of new olivine growing at the expense of orthopyroxene porphyroblast within a spinel-facies shear zone; (g) a reactive microtexture showing undeformed new olivine replacing exsolved clinopyroxene porphyroblast in a spinel-facies tectonite-mylonite shear zone; (h) reactive microtexture showing new olivine replacing kinked and exsolved orthopyroxene porphyroblast preserved in a spinel-facies tectonite-mylonite shear zone.

clusters previously described. At the microscale, olivine and pyroxene crystals show little or no optical evidence for internal strain. The granular lherzolites are frequently cut by spinel-bearing pyroxenite

bands that are locally folded and boudinaged. Albeit that the pyroxenites are folded, they never show an axial-plane structure; instead, the hinges of these folds are characterized by coarse-grained

spinel-bearing granoblastic textures. This structure clearly shows that annealing post-dates an earlier deformational (folding) event, which occurred under spinel-peridotite-facies conditions. In thin section, some samples of the mantle protoliths show clear microtextural features (pyroxene dissolution and new olivine crystallization) indicating that the rock was diffusely percolated under spinel-facies conditions by silica-undersaturated basaltic melts.

Spinel-facies shear zones: the mantle protolith is deformed by spinel-facies shear zones marked by the development of metre- to km-wide parallel bands of olivine + spinel tectonites and mylonites enclosing variable amounts of elongated and rotated sigmoidal porphyroclasts of pyroxene and orthopyroxene + spinel clusters with their microstructure inherited from the pristine lherzolites (Fig. 5b). Since in many outcrops a fine-grained mylonitic fabric is superimposed on a more coarse-grained tectonic deformation, presumably as a result of local high-strain accumulation, we describe structures associated with these tectonite and mylonite foliations together. In low-strain domains, pyroxenite layers occasionally show isoclinal folds with an axial-plane structure defined by the tectonite foliation (Fig. 4b). More commonly, the earlier pyroxenite layers are transposed, stretched and aligned along the high-strain tectonite–mylonite fabric (Fig. 4c), locally showing the development of asymmetrical boudinage. Orthopyroxene + spinel clusters are elongated with their long axes parallel to the tectonite–mylonite foliation, and, in some cases, are dismembered and recrystallized to fine-grained orthopyroxene + spinel granular aggregates, still preserving the shape of the original cluster. The sections parallel to the tectonite–mylonite foliation (*XY* planes) show cm-long ribbons of orthopyroxene defining a clear mineral lineation. In sections perpendicular to the tectonite–mylonite foliation and parallel to the mineral lineation (*XZ* planes), the orthopyroxene porphyroclasts show undulatory extinction, kink bands and resemble σ -type clasts, suggesting a component of simple shear during the deformation (Fig. 5c). Large orthopyroxene porphyroclasts preserve thin bands with granoblastic textures witnessing the early stage of annealing recrystallization under spinel-peridotite-facies conditions, which transformed the mantle protolith into granular lherzolites (Fig. 5d). Large olivine crystals, showing undulatory extinction, are rarely preserved but are substituted by smaller grains having a grain-shape fabric oblique to the main tectonite–mylonite foliation. Hoogerduijn Strating *et al.* (1993) demonstrated that the olivine [a] (*OkI*) lattice fabrics are also orientated oblique to the pyroxene foliation. The outer border of many pyroxene porphyroclasts consists of a fine-grained aggregate of granoblastic pyroxenes and

spinel, indicating that shearing occurred under spinel-facies conditions. Moreover, the matrix of the tectonite–mylonite shear zones is composed of fine- to ultrafine-grained aggregates of olivine + spinel. Accordingly, it can be concluded that spinel-facies shear zones were formed in the pristine granular/granoblastic lherzolites under spinel-peridotite-facies conditions.

Reactive structures within the spinel-facies shear zones. High-strain tectonites and mylonites host dm- to metre-scale bands of foliated spinel harzburgite and dunite parallel to the shear foliation (Fig. 4d, e). At the microscale, the spinel harzburgites show clearly reactive microstructures such as large deformed and kinked clino- and orthopyroxenes replaced by undeformed and optically homogeneous new olivine grains indicating pyroxene dissolution and olivine precipitation (Fig. 5e–h). In some cases, subeuhedral olivine grains crystallized within strongly deformed and exsolved orthopyroxene porphyroclasts. The dunite bands show olivine overgrowths and coarse-granular textures, suggesting that undersaturated basaltic melts infiltrated along pre-existing strongly deformed bands. As there is no evidence of any plagioclase among the crystallizing minerals, we infer that plagioclase was not stable in the system, hence that pressures were higher than 1.0 GPa. The above observations show that a first event of melt percolation by silica-undersaturated basaltic melts exploited, during their upward migration, the previously formed spinel-facies shear zones, and partly modified the structure and modal composition of the host peridotites. The progressive pyroxene dissolution and olivine precipitation (reactive phase) caused this melt to reach silica-saturation conditions under peridotite-spinel-facies conditions. In some outcrops, melt-free, spinel-facies shear zones show somewhat sharp contacts with almost isotropic granular, pyroxene-poor reactive spinel harzburgites (e.g. Piccardo & Vissers 2007) in which pyroxenes from the pyroxenite bands of the shear zones are dissolved and marked solely by alignments of spinel grains. At the microscale, these rocks are characterized by: (1) rims of new undeformed and optically homogeneous olivine grains replacing old and strained orthopyroxene crystals; (2) crystallization of subeuhedral unstrained olivine grains within kinked and exsolved orthopyroxene crystals; and (3) relicts of extremely exsolved and deformed clinopyroxene crystals surrounded by small grains of undeformed olivine. These structures demonstrate that silica-undersaturated melts were also infiltrated by porous flow reactive percolation (Piccardo & Vissers 2007), and were able to completely modify the structural and compositional characteristics of pre-existing melt-free,

spinel-facies shear zones. These relationships provide further support to the structural chronology of tectonic and magmatic events, since they indicate that the onset of melt-free extensional tectonics under spinel-facies conditions preceded decompression partial melting in the upwelling asthenosphere and the related infiltration of reactive melts through the deep mantle lithosphere. Local interstitial crystallization of small undeformed pyroxene grains in reactive spinel peridotites witnesses the attainment of silica-(pyroxene)-saturation conditions by the percolating melts. The huge, km-wide bodies of reactive spinel peridotites, which show almost isotropic granular textures (Piccardo & Vissers 2007), should represent former structured spinel-facies mantle lithosphere, bearing shear zones and percolation bands that were almost completely structurally and compositionally modified by the melt percolation under high melt/peridotite ratios and open-system conditions.

Impregnated plagioclase peridotites. Plagioclase-enriched granular peridotites: large volumes of spinel peridotite are locally replaced by plagioclase-enriched peridotites, in which the plagioclase concentration reaches values of 10–15% vol. The contacts between the two rock types are generally sharp, sometimes showing cm- to dm-wide bands of plagioclase-enriched peridotites running through the coarse granular reactive spinel peridotites. At the macroscale, the plagioclase-enriched peridotites can easily be distinguished by the diffuse presence of interstitial and unorientated plagioclase aggregates (Fig. 4f). In thin section, plagioclase crystals are frequently associated with orthopyroxene-originating rims and symplectitic coronas around the clinopyroxene porphyroclasts. New undeformed orthopyroxene grains, patches and veinlets replace the kinked mantle olivine. These microtextures have been interpreted as being the result of percolation and impregnation of silica-(orthopyroxene)-saturated melts that reacted with olivine and crystallized new orthopyroxene and plagioclase, due to increasing heat loss by conduction at plagioclase-facies conditions (Piccardo *et al.* 2004b). Locally, it is possible to observe that plagioclase + orthopyroxene assemblages formed in the interspace between spinel and olivine, with rims of plagioclase around spinel and rims of orthopyroxene around olivine crystals.

Plagioclase-enriched shear zones: in some outcrops, plagioclase-enriched peridotites were progressively transformed into high-strain plagioclase-bearing tectonites. These rocks clearly cut, at high angles, the earlier spinel tectonites–mylonites (Fig. 4g) and are characterized by the alignment of plagioclase crystals, strongly elongated and deformed along a new tectonic fabric. In thin

section, fresh magmatic plagioclase grains, characterized by clear polysynthetic twinning, occur as porphyroclasts aligned along a plagioclase-facies tectonite foliation (Fig. 6g, h). In some cases, mm-size gabbro-noritic pods crystallized in the cores of folded orthopyroxene crystals (Fig. 6a, b). Plagioclase crystals are often strongly altered and appear as brownish trails evidencing a plagioclase-bearing tectonic fabric. The chronological relationships between spinel-bearing and plagioclase-bearing tectonites are clearly observable close to the rims of old and deformed mantle orthopyroxene, where, moving away from the rim, the spinel-facies mineral assemblage is progressively replaced by a plagioclase-facies mineral association. Locally, the plagioclase-bearing shear zones overprint previous spinel aggregates still preserved within the pressure shadows of large orthopyroxene porphyroclasts (Fig. 6c, d).

Occasionally, the plagioclase-bearing shear zones overprint plagioclase-bearing aggregates previously grown at the outer border of pyroxene porphyroclasts (Fig. 6e, f).

The above observations lead us to suggest that at shallower depths, under plagioclase-facies conditions, spinel peridotites were percolated and impregnated by orthopyroxene-(silica)-saturated melts, transforming these rocks into plagioclase-enriched peridotites. The plagioclase-rich domains became the sites where new strain accumulated, such that the plagioclase-enriched peridotites, due to ongoing bulk extension, were progressively transformed into plagioclase-bearing peridotite tectonites and mylonites.

Replacive spinel dunites. Plagioclase-facies shear zones frequently host 1–20 m-scale bands of spinel dunite running parallel to the plagioclase-bearing foliation (concordant dunites, Fig. 4h). Locally, the dunite channels cut across pyroxenite-bearing tectonites (discordant dunites). In these cases, it can be observed that the spinel clinopyroxenites are progressively ‘dissolved’ within the dunite channels, where the clinopyroxenes are almost completely replaced by undeformed granular olivine. The continuity of the pyroxenite bands within the dunite channel is testified only by the presence of spinel trails, inherited from the previous spinel clinopyroxenite and running parallel to the shear foliation. These features clearly suggest a replacive origin of the spinel dunites (Boudier & Nicolas 1972; Boudier 1978). The fabric of the strongly deformed host tectonites and mylonites is completely recrystallized into a coarse granular texture in the dunites, mainly characterized by huge (over 1 cm in size) overgrown olivine crystals, which enclose elongated trains of spinel grains parallel to the foliation of the deformed country rocks. A

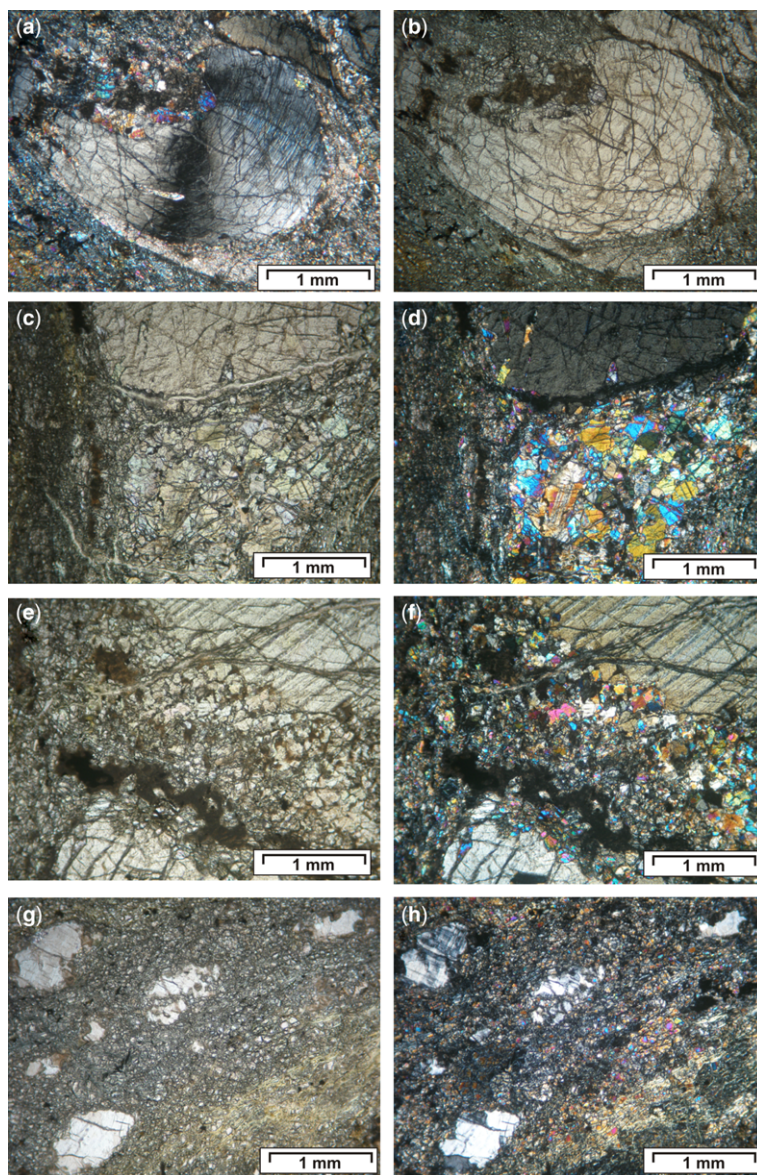


Fig. 6. Microstructures in tectonite–mylonite shear zones of the Erro–Tobbio peridotites from the study area. (a) & (b) Folded orthopyroxene porphyroclast in plagioclase-enriched shear zones showing the replacement by an almost undeformed, mm-size micro-gabbroic aggregate: plagioclase in the micro-gabbro is almost completely altered to a very fine dark brownish aggregate. (c) & (d) Orthopyroxene porphyroclast (upper part) showing a pressure shadow consisting of spinel-facies granoblastic aggregate (lower part), enclosed in a plagioclase-facies tectonite–mylonite shear zone. Note that plagioclase grains are completely altered to dark brownish aggregates. (e) & (f) Orthopyroxene porphyroclast (upper-right side) partly replaced by a plagioclase-rich microgranular aggregate in a plagioclase-enriched shear zone. Note that plagioclase grains are completely altered to dark brownish aggregates. (g) & (h) Plagioclase aggregates as porphyroclasts in a plagioclase-facies tectonite–mylonite shear zone.

typical microstructure of the spinel dunite consists of strongly deformed mantle olivine crystals replaced and overgrown by fine-grained aggregates of new,

almost undeformed, olivine grains. The occurrence of replacive spinel dunites suggests that a younger focused percolation of pyroxene undersaturated

melts, post-dating the diffuse porous flow percolation events responsible for both the reactive and the impregnated peridotites, produced either concordant or discordant replacive dunite bands.

Some relevant compositional characteristics

Mineral major- and trace-element compositions were carried out on samples of the different rock types described above.

Analytical methods. Major-element chemistry data of minerals in the selected samples were obtained at the Electron Microprobe Laboratory, University of Milano (Italy), using a JEOL 8200 Super Probe. Mineral analyses were always performed using detailed backscattered electron images to control the microstructural context. Trace elements in clinopyroxene, orthopyroxene and plagioclases were analysed using a laser ablation inductively coupled plasma (sector field) mass spectrometry (LA-ICP-(SF)MS) microprobe installed at the CNR-Istituto di Geoscienze e Georisorse, Section of Pavia. The LA-ICP-(SF)MS used is composed of a double-focusing sector field analyser (Finnigan Mat Element) coupled with a Q-switched Nd:YAG laser source (Quantel Brilliant). Full details of the analytical parameters and quantification procedures can be found in Tiepolo *et al.* (2002).

Representative mineral major-element compositions of clinopyroxenes, olivines, orthopyroxenes, plagioclases and spinels are reported in Tables 1–5. Representative mineral trace-element compositions of clinopyroxenes, orthopyroxenes and plagioclases are reported in Table 6.

Mineral major-element compositions. The clinopyroxenes from the oldest rock types (mantle protolith and spinel tectonites–mylonites) show relatively high Na and Al contents (Na_2O : 0.68–0.88 wt%; Al_2O_3 : 5.78–7.15 wt%). Two clinopyroxene groups can be identified within the reactive spinel harzburgites. The clinopyroxenes analysed in the harzburgite bands, parallel to the shear foliation (sample CM16 in Table 1), are still characterized by a high Na and Al content (Na_2O : 0.92–0.96 wt%; Al_2O_3 : 6.10–6.23 wt%). Those belonging to the massive spinel harzburgites (sample CM9 in Table 1) show a significant decrease both in Na and Al content (Na_2O : 0.40–0.43 wt%; Al_2O_3 : 4.57–5.98 wt%). The clinopyroxenes from the plagioclase-enriched shear zones show a similar Na content (Na_2O : 0.36–0.47 wt%), accompanied by a strong decrease in Al within the clinopyroxene rims and grains (Al_2O_3 : 3.18–3.50 wt%). The clinopyroxene cores from the plagioclase-enriched shear zones record a high Al content, with an average Al_2O_3 value of 7.36 wt%. The variation in Al content between cores

and rims of the same clinopyroxene crystals is common to all the rock types, with a higher Al content recorded by the cores and a lower Al content in the rims. The clinopyroxenes from the plagioclase-enriched peridotites also show a systematically higher Ti content (TiO_2 : 0.47–0.71 wt%) with respect to the other rock types (TiO_2 : 0.24–0.46 wt%). Plagioclase-enriched peridotites are characterized by a significantly higher TiO_2 concentration in spinel, with respect to the very low concentrations (maximum content of 0.12 wt%) in mantle spinel peridotites, that ranges from 0.34 to 0.38 wt% at increasing Cr#. It is widely accepted (i.e. Dick & Bullen 1984; Dick 1989; Hellebrand *et al.* 2002) that a high Ti content of spinel (i.e. $\text{TiO}_2 > 0.1$ wt%) in oceanic peridotites is a record of melt–peridotite interaction and indicates equilibration with MORB melts. Accordingly, a relatively high TiO_2 content in spinel from the Erro–Tobbio plagioclase peridotites confirms that they underwent reactive percolation of basaltic melts. Plagioclase in the studied Erro–Tobbio plagioclase-bearing peridotites is, moreover, strongly calcic, showing An% compositions varying in the range 86.1–90.3%.

Mineral trace-element compositions. All of the analysed samples of melt-interacted peridotites (i.e. mantle protoliths, massive spinel harzburgites, depleted harzburgites in spinel-facies shear zones, plagioclase-enriched shear zones and massive plagioclase peridotites) show strongly trace-element-depleted clinopyroxenes, which are characterized by highly light rare earth element (LREE) fractionated REE C1-chondrite normalized patterns (Fig. 7).

Plagioclase in plagioclase-bearing peridotites shows negative LREE fractionation (Fig. 7e). Interestingly, trace-element compositions and REE C1-chondrite normalized patterns do not show significant core–rim variations, except for the case of plagioclase-bearing peridotite CM3, where the Sr content slightly decreases from the core (0.95 ppm), which is most probably a remnant composition of a previous spinel-facies porphyroclast, to the rim (0.69 ppm), which is trace-element equilibrated with plagioclase. As a whole, it can be assumed that both core and rim in the same sample were trace-element equilibrated with the percolating melt. Plagioclase-bearing peridotites show a very low Sr and Zr content in clinopyroxenes (Sr in the range 0.64–0.95 ppm; Zr in the range 10.57–17.00 ppm) and very low Sr in plagioclase (Sr in the range 9.50–17.30 ppm). These compositional features are very similar to minerals from plagioclase-enriched peridotites and gabbro-norites from fossil and modern slow–ultraslow spreading oceans, but are significantly different to the same minerals crystallized by oceanic N-MORB (i.e. Hofmann 1988) (see the Discussion).

Table 1. Mineral major-element compositions (oxide wt%) of clinopyroxenes

Rock type	Melt-reacted mantle protolith				Spinel mylonite		Reactive spinel harzburgites					Plagioclase peridotites	
Sample	TG4		TG5		CM2		CM16		CM17	CM9		CM3	
Structural site	Porph* Core (6 [†])	Porph Rim (3)	Porph Core (2)	Porph Rim (1)	Porph Core (3)	Porph Rim (4)	Porph Core (3)	Porph Rim (1)	Porph Core (3)	Porph Core (2)	Porph Rim (2)	Porph Core (5)	Porph Rim (3)
SiO ₂	50.78	50.84	50.99	51.14	50.20	50.85	51.61	52.16	51.16	49.87	51.16	49.80	51.83
TiO ₂	0.30	0.29	0.30	0.39	0.42	0.46	0.24	0.27	0.37	0.30	0.30	0.47	0.65
Al ₂ O ₃	7.01	5.86	6.16	5.78	7.15	6.03	6.23	6.10	7.40	5.98	4.57	7.36	3.50
Cr ₂ O ₃	1.16	0.90	1.34	1.16	0.95	0.78	1.35	1.35	0.99	1.17	0.76	0.87	0.78
FeO	2.78	2.76	2.70	2.75	3.08	2.91	2.57	2.75	2.83	2.75	2.68	3.11	2.64
MnO	0.10	0.09	0.07	0.06	0.07	0.10	0.08	0.10	0.09	0.09	0.07	0.11	0.10
MgO	14.85	15.66	14.77	14.98	15.81	15.82	15.10	17.33	14.57	15.28	15.92	15.07	16.40
NiO	0.05	0.00	0.05	0.03	0.09	0.03	0.06	0.00	0.05	0.07	0.03	0.05	0.06
CaO	21.75	21.76	22.13	22.34	20.44	21.23	21.58	19.25	22.12	22.81	23.07	22.37	22.95
Na ₂ O	0.81	0.68	0.85	0.88	0.84	0.80	0.96	0.92	0.85	0.43	0.40	0.47	0.36
K ₂ O	0.00	0.00	0.02	0.00	0.00	0.00	0.00	0.00	0.00	0.00	0.00	0.01	0.00
Total	99.57	98.84	99.37	99.52	99.05	99.00	99.79	100.23	100.45	98.73	98.95	99.69	99.26
Al (×100)	30.10	25.30	26.60	24.90	30.80	25.90	26.70	25.90	31.60	26.00	19.80	31.70	15.10
Na (×100)	5.72	4.82	6.06	6.24	5.95	5.67	6.80	6.40	5.99	3.10	2.85	3.34	2.55
Mg# (×100)	91.20	93.20	91.50	93.00	93.50	93.80	90.80	91.90	90.50	95.40	94.70	92.80	93.30

*Porph, porphyroclast.

[†]Values in parentheses indicate the averaged number of analyses.

Table 2. Mineral major-element compositions (oxide wt%) of olivines

Rock type	Mantle protolith		Spinel mylonite	Reactive spinel harzburgites					Plagioclase peridotite
Sample	TG4	TG5	CM2	CM9			CM16	CM17	CM3bis
Structural site	Grain (3 [†])	Porph* Core (3)	Grain (2)	Porph Core (3)	Porph Rim (3)	Grain (5)	Grain (1)	Grain (4)	Grain (2)
SiO ₂	40.60	40.85	40.54	40.65	40.19	40.58	40.69	41.21	40.79
TiO ₂	0.02	0.00	0.00	0.01	0.01	0.01	0.01	0.01	0.02
Al ₂ O ₃	0.00	0.01	0.01	0.00	0.01	0.00	0.03	0.01	0.00
Cr ₂ O ₃	0.02	0.02	0.00	0.03	0.04	0.01	0.00	0.04	0.02
FeO	9.68	9.53	9.38	9.43	9.38	9.41	9.02	9.53	9.59
MnO	0.12	0.14	0.11	0.13	0.15	0.15	0.11	0.14	0.14
MgO	48.59	48.86	49.48	50.18	49.21	50.05	48.17	49.13	50.21
NiO	0.37	0.42	0.37	0.38	0.45	0.37	0.43	0.41	0.41
CaO	0.00	0.01	0.05	0.01	0.01	0.01	0.01	0.01	0.01
Na ₂ O	0.01	0.01	0.00	0.00	0.00	0.00	0.00	0.01	0.01
K ₂ O	0.00	0.00	0.00	0.00	0.00	0.00	0.00	0.01	0.00
Total	99.42	99.85	99.92	100.84	99.45	100.60	98.47	100.52	101.19
Fo%	89.95	90.14	90.39	90.46	90.34	90.46	90.49	90.18	90.32

*Porph, porphyroclast.

[†]Values in parentheses indicate the averaged number of analyses.

Table 3. Mineral major-element compositions (oxide wt%) of orthopyroxenes

Rock type	Mantle protolith		Spinel mylonite			Reactive spinel harzburgites						Plagioclase peridotites		
Sample	TG5		CM2			CM9			CM16	CM17		CM3		CM3bis
Structural site	Porph* Core (7 [†])	Porph Rim (1)	Porph Core (3)	Porph Rim (5)	Cluster (3)	Porph Core (6)	Porph Rim (2)	Grain (1)	Porph Core (3)	Porph Core (3)	Porph Rim (3)	Porph Core (6)	Porph Rim (2)	Grain (2)
SiO ₂	54.37	54.51	53.38	54.30	55.13	54.37	55.14	54.96	54.96	54.37	55.01	54.36	55.01	56.36
TiO ₂	0.08	0.10	0.15	0.13	0.09	0.11	0.09	0.10	0.12	0.15	0.12	0.19	0.22	0.19
Al ₂ O ₃	4.85	4.68	5.90	4.18	3.52	4.42	3.91	3.90	5.12	5.08	4.00	4.42	2.61	1.87
Cr ₂ O ₃	0.78	0.79	0.08	0.07	0.06	0.65	0.56	0.33	0.90	0.50	0.40	0.76	0.56	0.36
FeO	6.18	5.97	6.22	6.36	6.47	6.22	6.30	6.35	5.43	6.48	6.89	6.54	6.68	6.69
MnO	0.12	0.16	0.11	0.16	0.14	0.16	0.15	0.11	0.09	0.15	0.14	0.15	0.17	0.13
MgO	31.91	31.62	31.96	32.65	33.25	32.87	32.97	33.42	29.82	31.70	33.29	32.63	33.29	34.56
NiO	0.08	0.05	0.08	0.07	0.06	0.12	0.11	0.04	0.12	0.07	0.12	0.06	0.10	0.11
CaO	0.88	1.10	0.85	0.93	0.62	0.82	1.12	0.69	3.29	1.55	0.68	0.94	0.71	0.67
Na ₂ O	0.05	0.03	0.04	0.04	0.04	0.02	0.03	0.02	0.19	0.08	0.03	0.02	0.03	0.01
K ₂ O	0.00	0.00	0.01	0.00	0.00	0.00	0.00	0.00	0.01	0.00	0.00	0.00	0.01	0.00
Total	99.30	99.01	99.28	99.18	99.62	99.76	100.38	99.91	100.06	100.14	100.68	100.07	99.37	100.95

*Porph, porphyroclast.

[†]Values in parentheses indicate the averaged number of analyses.

Table 4. Mineral major-element compositions (oxide wt%) of plagioclases

Rock type	Plagioclase peridotites											
Sample	CM3							CM3bis				
Structural site	Porph* Core	Porph Core	Porph Core	Porph Core	Porph Rim	Porph Rim	Porph Rim	Porph Core	Porph Core	Porph Core	Porph Rim	Porph Rim
SiO ₂	45.87	46.13	46.25	46.41	46.07	46.06	46.77	46.09	45.55	45.72	46.30	46.93
TiO ₂	0.06	0.00	0.00	0.02	0.00	0.01	0.02	0.01	0.02	0.01	0.01	0.04
Al ₂ O ₃	35.21	35.21	35.29	34.72	35.27	35.01	34.52	34.99	35.45	34.87	34.98	34.32
Cr ₂ O ₃	0.00	0.05	0.00	0.00	0.00	0.00	0.00	0.03	0.01	0.00	0.00	0.05
FeO	0.05	0.12	0.02	0.06	0.23	0.18	0.21	0.11	0.12	0.17	0.23	0.24
MnO	0.00	0.00	0.00	0.00	0.00	0.00	0.00	0.00	0.02	0.00	0.00	0.06
MgO	0.00	0.00	0.01	0.00	0.01	0.01	0.00	0.00	0.01	0.01	0.08	0.01
NiO	0.01	0.06	0.02	0.02	0.00	0.03	0.00	0.00	0.00	0.02	0.06	0.03
CaO	17.94	17.78	17.49	17.34	17.56	17.77	17.25	17.75	18.03	17.81	18.02	17.29
Na ₂ O	1.25	1.43	1.55	1.44	1.43	1.34	1.54	1.23	1.08	1.23	1.08	1.44
K ₂ O	0.00	0.00	0.00	0.02	0.00	0.02	0.00	0.00	0.03	0.00	0.00	0.00
Total	100.39	100.78	100.64	100.02	100.58	100.43	100.30	100.21	100.31	99.85	100.76	100.41
An%	88.8	87.3	86.2	86.9	87.2	88.0	86.1	88.9	90.3	88.9	90.2	86.9

*Porph, porphyroclast.

Table 5. Mineral major-element compositions (oxide wt%) of spinels

Rock type	Mantle protolith		Spinel mylonite			Reactive spinel harzburgites			Plagioclase peridotites		
Sample	TG5		CM2			CM9	CM17		CM3–CM3bis		
Structural site	Cluster Core (2 [†])	Cluster Rim (1)	Cluster Core (3)	Cluster Rim (1)	Grain (6)	Porph* Core (7)	Cluster Core (1)	Cluster Rim (1)	Porph Core (2)	Porph Rim (2)	Grain (2)
SiO ₂	0.00	0.00	0.01	0.00	0.04	0.04	0.05	0.10	0.03	0.06	0.06
TiO ₂	0.07	0.04	0.09	0.04	0.04	0.07	0.12	0.08	0.34	0.38	0.38
Al ₂ O ₃	55.52	51.91	55.42	53.68	56.23	51.20	56.99	57.40	36.39	32.73	34.30
Cr ₂ O ₃	11.92	14.53	12.07	13.40	11.70	15.08	12.61	12.65	29.21	32.21	28.95
FeO	11.78	12.72	11.65	12.38	11.86	15.14	12.21	11.93	18.82	20.15	23.61
MnO	0.06	0.10	0.08	0.10	0.06	0.13	0.05	0.05	0.04	0.10	0.17
MgO	19.96	19.48	20.19	19.35	19.78	17.74	19.00	17.40	15.35	14.38	11.90
NiO	0.33	0.27	0.35	0.29	0.33	0.31	0.42	0.33	0.17	0.24	0.12
CaO	0.00	0.00	0.01	0.01	0.01	0.01	0.01	0.47	0.01	0.01	0.01
Na ₂ O	0.00	0.04	0.01	0.02	0.03	0.01	0.01	0.00	0.01	0.01	0.03
K ₂ O	0.00	0.00	0.00	0.00	0.00	0.00	0.00	0.00	0.01	0.00	0.00
Total	99.64	99.09	99.89	99.26	100.06	99.74	101.47	100.41	100.39	100.26	99.51
Mg# (×100)	78.30	78.10	79.60	76.00	77.40	71.50	73.70	69.10	65.25	62.40	52.50
Cr# (×100)	12.58	15.81	12.85	12.92	12.25	16.51	12.90	12.90	35.00	39.77	36.15

*Porph, porphyroclast.

[†]Values in parentheses indicate the averaged number of analyses.

Table 6. Mineral trace-element compositions (ppm)

Rock type	Mantle protolith				Spinel-facies shear zones			Reactive spinel harzburgites (bands)						
Sample	TG5				CM2			CM16			CM17			
Mineral* Site	cpx Core	cpx Rim	opx Core	opx Rim	cpx Core	cpx Rim	opx Core	cpx Core	cpx Rim	opx Core	cpx Core	cpx Rim	opx Cluster	opx Cluster
La	0.05	0.07	0.01	–	0.03	0.02	–	0.08	0.09	–	0.02	0.03	–	–
Ce	0.61	0.62	0.01	0.01	0.38	0.37	0.01	0.63	0.64	0.02	0.38	0.37	–	–
Pr	0.20	0.25	0.00	0.01	0.19	0.19	0.01	0.20	0.23	0.01	0.16	0.17	–	–
Nd	2.09	2.12	0.04	0.11	1.49	1.59		1.62	1.55	0.05	1.79	1.82	0.01	–
Sm	1.17	0.93	0.03	0.03	1.17	1.02	0.03	0.80	0.99	0.03	1.22	1.25	–	0.04
Eu	0.46	0.51	0.03	0.03	0.50	0.54	0.02	0.47	0.47	0.03	0.50	0.52	0.01	0.02
Gd	1.58	1.46	0.09	0.10	2.12	1.88	0.07	1.70	1.77	0.08	2.02	1.92	0.05	0.07
Tb	0.31	0.29	0.03	0.03	0.41	0.34	0.03	0.32	0.32	0.02	0.40	0.37	0.01	0.01
Dy	2.06	2.17	0.22	0.13	2.95	2.83	0.21	2.26	2.29	0.26	2.95	2.68	0.21	0.21
Er	1.16	1.51	0.18	0.45	1.92	1.70	0.33	1.33	1.35	0.22	1.51	1.95	0.22	0.23
Tm	0.19	0.18	0.03	0.05	0.28	0.23	0.06	0.19	0.18	0.02	0.23	0.27	0.05	0.05
Yb	0.99	1.41	0.25	0.33	1.81	1.94	0.44	1.32	1.12	0.27	1.66	1.60	0.32	0.50
Lu	0.18	0.15	0.06	0.06	0.23	0.22	0.08	0.16	0.17	0.04	0.25	0.23	0.09	0.11
Sr	6.22	16.75	0.40	0.12	4.99	5.27	0.06	7.41	6.65	0.15	4.34	4.43	0.09	0.10
Zr	6.11	6.37	0.97	0.93	7.17	7.55	0.99	7.89	7.69	1.22	6.80	6.81	0.60	0.63
Y	11.24	11.36	1.59	1.49	16.12	15.74	1.73	13.60	12.51	1.62	15.79	15.72	1.43	1.92
Sc	51.84	55.92	25.51	27.35	52.62	50.64	24.12	53.03	52.91	22.93	51.73	52.03	22.64	26.00
V	254	256	120	126	265	244	111	245	234	114	277	267	114	130
Cr	9072	10 043	4770	5024	6661	5457	2797	9864	8526	5648	7337	6807	2523	2828

Rock type	Reactive spinel harzburgite (massive)				Plagioclase peridotite				Plagioclase-bearing tectonites					
Sample	CM9				ETR22 [†]				CM3					
Mineral* Site	cpx Core	cpx Rim	cpx Core	cpx Rim	cpx Core	cpx Rim	opx Core	plg	cpx Core	cpx Rim	opx Core	plg	plg	plg
La	0.01	0.01	0.01	0.01	–	–	–	–	0.02	0.03	–	0.01	0.02	0.04
Ce	0.17	0.16	0.15	0.17	0.64	0.53	0.05	0.14	0.51	0.57	0.02	0.18	0.22	0.24
Pr	0.07	0.09	0.08	0.06	–	–	–	–	0.22	0.28	0.01	0.04	0.05	0.06
Nd	1.02	0.90	0.93	0.82	3.40	4.20	0.08	0.22	2.47	2.81	0.09	0.28	0.34	0.34
Sm	0.77	0.78	0.77	0.63	2.32	2.38	0.08	0.10	1.72	2.00	0.08	0.13	0.07	0.10
Eu	0.33	0.50	0.32	0.31	0.89	0.86	0.04	0.35	0.67	0.64	0.04	0.35	0.31	0.36
Gd	1.36	0.97	1.31	1.16	4.20	5.20	0.39	–	2.51	3.17	0.16	0.07	0.09	0.06
Tb	0.32	0.30	0.32	0.27	–	–	–	–	0.57	0.64	0.05	0.01	0.01	0.01
Dy	2.27	2.47	2.35	2.12	5.40	6.10	0.66	0.07	3.97	4.37	0.50	–	0.03	0.06
Er	1.48	1.17	1.62	1.40	2.96	2.93	0.43	–	2.19	2.63	0.47	–	0.03	–
Tm	0.21	0.25	0.21	0.20	–	–	–	–	0.33	0.37	0.07	–	0.01	–
Yb	1.24	1.30	1.48	1.45	3.50	3.10	0.77	–	2.03	2.44	0.48	–	0.04	–
Lu	0.18	0.17	0.19	0.18	–	–	–	–	0.35	0.32	0.11	0.01	–	0.01
Sr	2.92	2.37	3.58	5.48	0.82	0.88	0.07	9.50	0.95	0.69	0.24	17.30	11.29	11.73
Zr	3.31	3.30	3.26	3.17	13.00	17.00	2.30	0.05	10.61	11.94	2.23	0.05	0.04	–
Y	12.78	12.26	12.57	11.75	32.00	34.00	4.30	0.25	22.01	24.50	3.30	0.28	0.27	0.22
Sc	50.60	47.38	50.58	49.59	58.00	71.00	29.00	1.00	60.14	61.15	32.47	1.57	1.43	1.35
V	257	250	262	259	327	387	206	2.20	317	325	161	2.29	0.92	1.21
Cr	7390	7051	7477	6849	5781	6990	4329	1.00	6794	6971	4196	206	2.03	2.11

*cpx, clinopyroxene; opx, orthopyroxene; plg, plagioclase.

[†]Data from Romairone (1999).

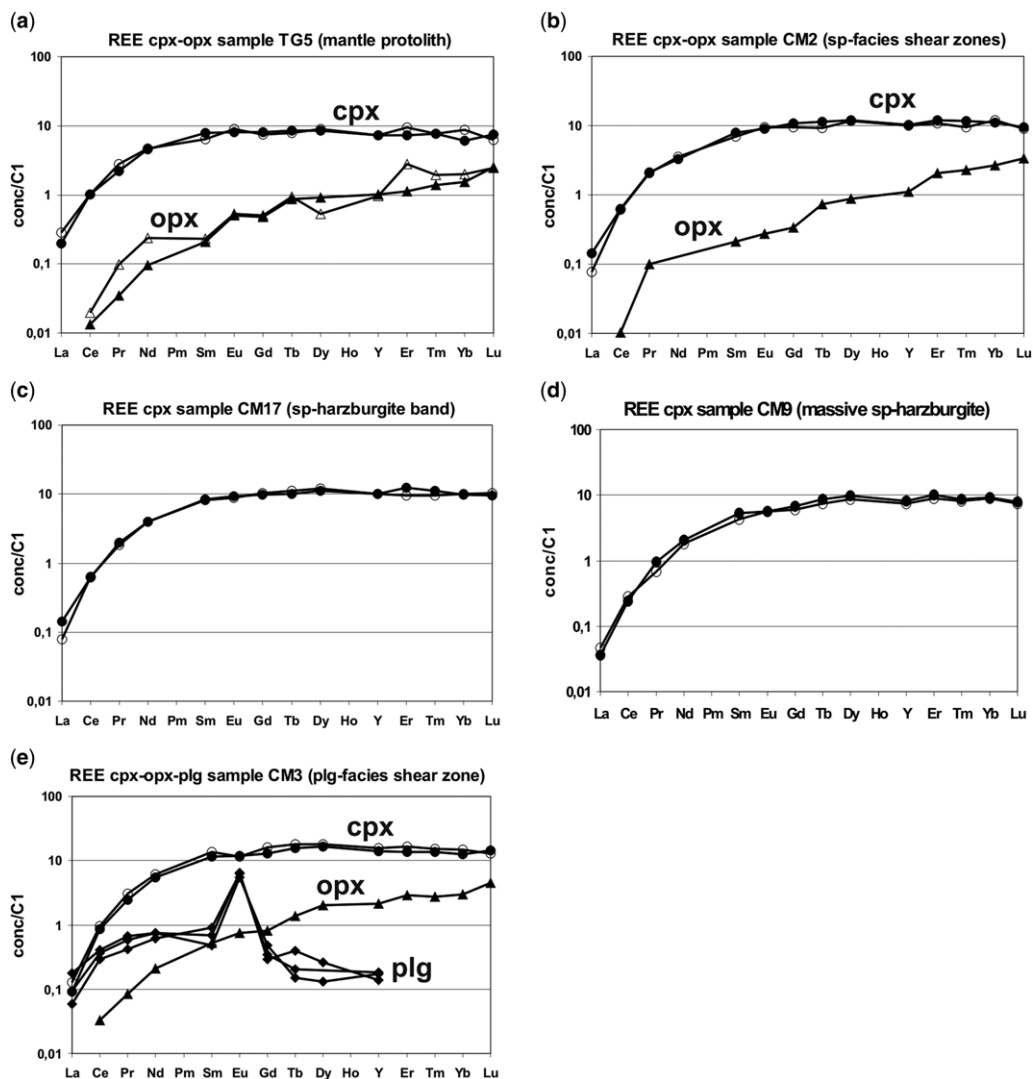


Fig. 7. C1-chondrite-normalized REE patterns of cores (full symbols) and rims (open symbols) of clinopyroxenes, orthopyroxenes and plagioclases from representative samples of: (a) the mantle protolith (with orthopyroxene); (b) spinel-facies tectonite–mylonite shear zones (with orthopyroxene); (c) reactive spinel-harzburgite-band spinel-facies tectonite–mylonite shear zones; (d) massive reactive spinel harzburgites; (e) plagioclase-facies shear zone (with plagioclase and orthopyroxene). Note that the core and rim compositions are practically coincident in the same sample, and that plagioclase is strongly fractionated in the LREE.

Discussion

As previously discussed, our work deals with the tectonic–magmatic evolution of subcontinental mantle as recorded by the N to NE bodies of the Ero–Tobbio peridotite, which have been considered to be located in a marginal (OCT) setting of the basin, and preserve the oldest structural records: that is, spinel(ex-garnet) protoliths, melt-free and melt-bearing shear zones, as well as

structural relationships between the effects of dry extension and early melt infiltration.

Structural chronology of tectonic–magmatic events

The structural, petrological and geochemical data reported in the previous sections enable us to assess the complex tectonic–magmatic evolution recorded by the Ero–Tobbio peridotites during the rifting to

spreading evolution of the Ligurian Tethys. The tectonic evolution of the structurally oldest rock type recognized in the study area (namely, the mantle protolith) is difficult to unravel on the basis of structural observations alone, since a diffuse annealing stage led to a complete recrystallization to granular textures. Nevertheless, the mantle protolith is characterized by the occurrence of numerous clusters of orthopyroxene + spinel, which have been interpreted as subsolidus microstructures testifying to the breakdown of pre-existing mantle garnets (Hoogerduijn Strating *et al.* 1993). The Erro–Tobbio mantle protolith thus contains evidence for the exhumation from garnet- to spinel-facies conditions. Despite the absence of geochronological constraints on this specific process, it is reasonable to hypothesize that this uplift, from garnet- to spinel-facies conditions, occurred during the earliest rifting stages in the Ligurian Tethys domain, most probably between 225 and 190 Ma (Müntener & Hermann 2001; Capitanio & Goes 2006; Montanini *et al.* 2006). The Mesozoic extension is constrained in extensional shear zones by Lu–Hf isochrones (minimum age of 220 ± 13 Ma) in External Liguride pyroxenites (Montanini *et al.* 2006) and $^{40}\text{Ar}/^{39}\text{Ar}$ ages (225 Ma) of amphiboles from the Malenco peridotites (Müntener & Hermann 2001). These latter authors emphasized that: ‘these shear zones formed during exhumation of the lower crust and upper mantle and are related to early rifting of the Adriatic passive continental margin’ (Müntener & Hermann 2001, p. 267).

Previous field and microstructural studies (Drury *et al.* 1990; Hoogerduijn Strating *et al.* 1990, 1993; Vissers *et al.* 1991), and new detailed field investigations, revealed that the mantle protolith has been deformed by up to km-scale shear zones that developed a tectonic–mylonitic foliation under spinel-peridotite-facies conditions. The observation, at both the macro- and microscale, of numerous sigmoidal porphyroclasts deformed and rotated along the main foliation surface suggests that these zones accommodated an important component of simple shear. This is corroborated by the evidence that the olivine grains often define an oblique foliation (both grain shape and lattice fabric: Hoogerduijn Strating *et al.* 1993) with respect to the main foliation plane. Some domains of sheared Erro–Tobbio peridotite do not show records of melt–peridotite interaction, and allow description of the fully melt-free tectonic–metamorphic subsolidus evolution of the subcontinental mantle of the Adria margin, which escaped melt percolation and was only percolated at very shallow levels by the downward infiltration of continental or oceanic hydrous fluids (Drury *et al.* 1990; Vissers *et al.* 1991; Hoogerduijn Strating *et al.* 1990, 1993), which formed hydrous (i.e. chlorite- and amphibole-

bearing) syntectonic assemblages. In several outcrops, decimetre- to metre-scale bands of reactive spinel harzburgites and dunites run parallel to the tectonic–mylonitic foliation. These features clearly indicate that pyroxene(silica)-undersaturated melts infiltrated along the pre-existing spinel-facies shear zones via channelled porous flow, and exploited the foliation structures for their upward migration. During their ascent, the melts produced visible textural and compositional effects in the host tectonites–mylonites, causing their progressive pyroxene depletion and microstructural change. At this stage, we note that for partial melting to occur under almost adiabatic decompression due to passively upwelling asthenosphere, continental extension must have thinned the lithosphere by a factor of around 2 (i.e. the lithosphere must have thinned to half of its original thickness: Foucher *et al.* 1982; Corti *et al.* 2007; Ranalli *et al.* 2007; Piccardo *et al.* 2009). It is likely, therefore, that the lithosphere was first thinned via the development of early melt-free shear zones and that this deformed lithosphere was subsequently infiltrated by reactive melts, produced by the partial melting of the underlying asthenosphere, migrating along the pre-existing extensional shear zones and percolating by diffuse porous flow through the host peridotite.

Field relationships reveal that large portions of spinel peridotites are locally replaced by plagioclase-enriched peridotites. These rocks are characterized by interstitial crystallization of up to 10–15% by a volume of unorientated plagioclase crystals. Crystallization of plagioclase, replacement of orthopyroxene on mantle olivine and formation of mm-size gabbro-norite pods indicate that orthopyroxene(-silica)-saturated melts percolated, impregnated and crystallized interstitial gabbro-norite minerals due to increasing heat loss by conduction at these shallow mantle levels (Piccardo *et al.* 2004b).

Plagioclase-bearing tectonite shear zones cutting through the plagioclase-enriched peridotites clearly formed later. Numerous granoblastic aggregates of previous magmatic plagioclase occur as clasts along this new tectonite fabric. The plagioclase-bearing shear zones clearly post-date the spinel tectonites–mylonites and reflect younger deformation events that occurred at shallow levels in the lithospheric mantle ($P < 1.0$ GPa, plagioclase-peridotite-facies conditions).

The last magmatic event is represented by the formation of dunite channels by the focused migration of reactive melts along compositional/structural discontinuities, which both cut and follow previous plagioclase-facies shear zones. Open-system migration and high melt/rock ratios produced the almost complete dissolution of pyroxenes (and, eventually, plagioclase) in the host peridotites,

forming high-porosity, high-permeability channels that were exploited for rapid upwelling of melts from the asthenosphere without significant interaction with the host peridotite. As recognized from interstitial and megacrystic clinopyroxenes, sporadically associated with plagioclase in these dunite channels, the percolating liquids were aggregated MORB melts, very similar to the MORB of Hofmann (1988), recognized as the primary/parental liquids of the oceanic magmatism (olivine-gabbro intrusions and basaltic volcanics) (e.g. Piccardo 2003; Piccardo & Vissers 2007; Piccardo *et al.* 2007, 2009).

Inferences on the compositions of the percolating melts

Whilst the clinopyroxene modal content is highly variable in one and the same depleted spinel-peridotite body or shear-zone band (from >2 to 8 vol%), clinopyroxenes show a remarkable homogeneity in their trace-element compositions. This leads us to suggest that clinopyroxenes from these peridotites were trace-element equilibrated with the percolating melt, whereas the clinopyroxene modal compositions depend on the degree of pyroxene reactive dissolution during melt–rock interaction (Piccardo & Vissers 2007 and references therein). The liquids that percolated through the

Erro–Tobbio spinel peridotites most probably represented the early primary melts migrated from the asthenosphere. We therefore assume that calculated equilibrium liquids with the peridotite clinopyroxenes, equilibrated with the percolated melt, can provide significant insights into the trace-element compositions of the primary melts percolated from the asthenosphere. With this notion in mind, we calculated the REE composition of liquids in equilibrium with the early melt-interacted spinel peridotite (CM9: massive spinel harzburgite) to obtain information on the primary characteristics of the percolating asthenospheric melts. The calculated equilibrium liquid compositions (using cpx–liquid partition coefficients appropriate for high-temperature, silica-undersaturated systems: e.g. Hart & Dunn 1993; Ionov *et al.* 2002) have been compared with the REE compositions of single-melt increments produced by a fractional melting process (Johnson *et al.* 1990), starting from the depleted MORB mantle (DMM) source of Johnson *et al.* (1990). The C1-normalized REE patterns of melts in equilibrium with clinopyroxenes show a good match with the compositions of depleted single-melt increments after about 5–6% fractional melting of a spinel-facies DMM source (Fig. 8a).

Plate Model numerical simulations (applying the method of Vernières *et al.* 1997) have been performed (e.g. Piccardo *et al.* 2007) with the aim of

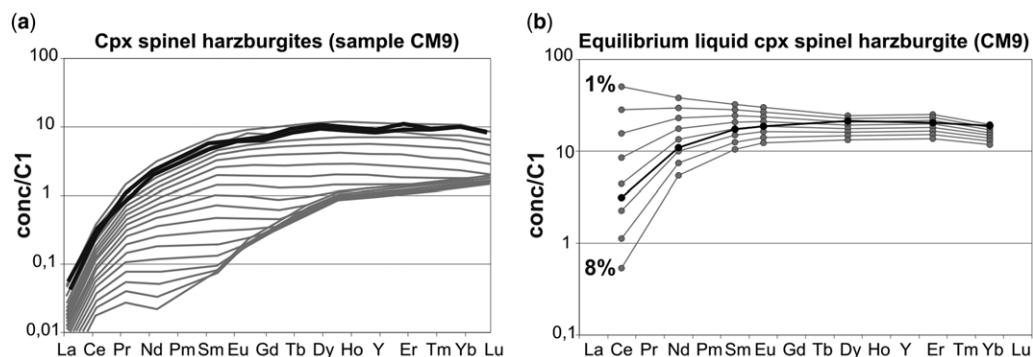


Fig. 8. Evaluation of the liquid in equilibrium with the clinopyroxene of a representative sample of Erro–Tobbio reactive spinel harzburgite. (a) Plate Model numerical simulations (applying the method of Vernières *et al.* 1997) were performed with the aim of understanding the nature of the percolating melts, and the chemical and physical parameters governing their interaction with the ambient peridotite. A refractory residuum after 20% fractional melting of spinel-facies DMM was used as ambient peridotite, and those produced by 5–7% fractional melting of a spinel-facies DMM source as injected melts. The Plate Model numerical simulations indicate that the REE pattern of the CM9 clinopyroxene is almost coincident with modelled REE patterns of clinopyroxene fully equilibrated with the percolating melt used in the simulation. (b) The liquid composition calculated in equilibrium with the clinopyroxene (using cpx–liquid partition coefficients appropriate for high-temperature, silica-undersaturated systems: e.g. Hart & Dunn 1993; Ionov *et al.* 2002) is compared with the REE compositions of single-melt increments produced by a fractional melting process (Johnson *et al.* 1990), starting from the DMM source of Johnson *et al.* (1990). The C1-normalized REE patterns of melts in equilibrium with clinopyroxenes match well the compositions of depleted single-melt increments after about 5–6% fractional melting of a spinel-facies DMM source.

understanding the nature of the percolating melts, and the chemical and physical parameters governing their interaction with the ambient peridotite. In all the specific numerical simulations, a refractory residuum after 20% fractional melting of spinel-facies DMM has been used as the ambient peridotite (see Piccardo *et al.* 2007 for more discussion). The model is capable of approaching the geochemical features of the LREE-fractionated clinopyroxenes, using as injected melts those produced by 5–7% fractional melting of a spinel-facies DMM source. The Plate Model numerical simulations indicate that the REE pattern of the CM9 clinopyroxene is almost coincident with modelled REE patterns of clinopyroxene fully equilibrated with the percolating melt used in the simulation (Fig. 8b). In summary, all of the data suggest that clinopyroxenes from the reactive spinel peridotites were almost completely equilibrated with percolating melts, which were produced as single-melt increments by low degrees (around 5–6%) of partial melting of a spinel-facies DMM source.

The peritectic reaction of original silica-undersaturated liquids with mantle pyroxenes during porous melt percolation (e.g. Kelemen *et al.* 1995) progressively led to silica(orthopyroxene)-saturation of the melt, because of increasing pyroxene dissolution into the reacting melt (as suggested by Kelemen *et al.* 1997; Dijkstra *et al.* 2003). In fact, as evidenced by Kelemen and coworkers (Kelemen *et al.* 1992, 1995), liquid rising adiabatically from the asthenosphere is above its liquidus temperature. For this reason, the melt initially dissolves peridotite. This leads to olivine saturation in the liquid, which will crystallize olivine and continue to dissolve pyroxene.

Accordingly, the silica-saturated basaltic melts that impregnated plagioclase peridotites and crystallized gabbro-norite pods were ‘derivative’ liquids, formed by melt–peridotite reactive interaction (in the sense of Kelemen 1990; Cann *et al.* 1999; and references therein), which were produced by progressive silica-saturation of primary silica-undersaturated melt increments due to pyroxene dissolution and olivine precipitation during melt-reactive percolation (see Piccardo *et al.* 2014).

According to Kelemen *et al.* (1997) and Dijkstra *et al.* (2003), these modified percolating melt fractions may travel by porous flow, leading to extensive melt–rock reaction and refertilization at shallow, plagioclase-facies, mantle levels. Upon reaching the crystallization temperature, the liquid composition should be saturated in pyroxenes and be similar in major-element composition (Mg/Fe, Ni, Cr, SiO₂) to a small degree of low-pressure melting (i.e. 0.5 GPa) of mantle lherzolites, although its trace-element characteristics may preserve a ‘memory’ of its open-system provenance (Kelemen

et al. 1995). The high Mg#, Cr and Ni content of melt-equilibrated pyroxenes evidence that the percolated derivative liquids cannot be fractionated melts. Their SiO₂ content is significantly high because of dissolution and melt incorporation of silica-saturated mantle pyroxenes and deposition of olivine, and their open-system provenance (i.e. their provenance from the early depleted melt fractions that percolated under spinel-facies conditions) is testified to by the very low incompatible trace-element content of plagioclases and clinopyroxenes. These compositional characteristics, together with microtextural data, demonstrate their direct link with the primary depleted single-melt increments that, at an early stage, infiltrated the lower lithosphere under spinel-facies conditions, forming reactive spinel peridotites.

On binary diagrams for discriminant compositional parameters of clinopyroxenes and plagioclase (Fig. 9) from the Erro–Tobbio plagioclase peridotites, the representative points of the analysed minerals fall within the field of minerals of plagioclase-enriched peridotites and gabbro-norites from fossil (ophiolite massifs of the Ligurian Tethys) and modern (Gakkel Ridge, SW Indian Ridge (SWIR), Mid-Atlantic Ridge (MAR)) slow–ultraslow spreading oceans. These rocks crystallized from silica-saturated, strongly depleted MORB-type melts (see the discussions in Piccardo & Guarnieri 2011; Piccardo *et al.* 2014).

Accordingly, these melts pertain to the strongly trace-element-depleted, silica-saturated ‘hidden magmatism’, which caused melt stagnation and thermal erosion of the shallow asthenosphere during the rifting stages of slow–ultraslow spreading oceans (see Piccardo & Guarnieri 2011; Piccardo *et al.* 2014). These data reinforce the evidence that fossil and modern slow–ultraslow spreading oceans are characterized by early stagnation and crystallization of strongly trace-element-depleted, silica-saturated melts, which never reached the seafloor and show significant compositional differences from the later oceanic aggregated MORB melts, which gave rise to olivine-gabbro intrusions, olivine-rich troctolites of oceanic core complexes (OCC) and basaltic volcanics (see the discussion in Piccardo *et al.* 2014).

Therefore, we conclude that melts infiltrating and percolating along the extensional shear zones of the Erro–Tobbio peridotites formed wide replacive channels for further melt migration from spinel- to plagioclase-facies conditions within the extending subcontinental lithosphere. During this migration, which was accompanied by large replacements of the host peridotites by reactive harzburgites and, at shallower levels, by plagioclase-enriched peridotites, melt–peridotite interactions modified the compositional and

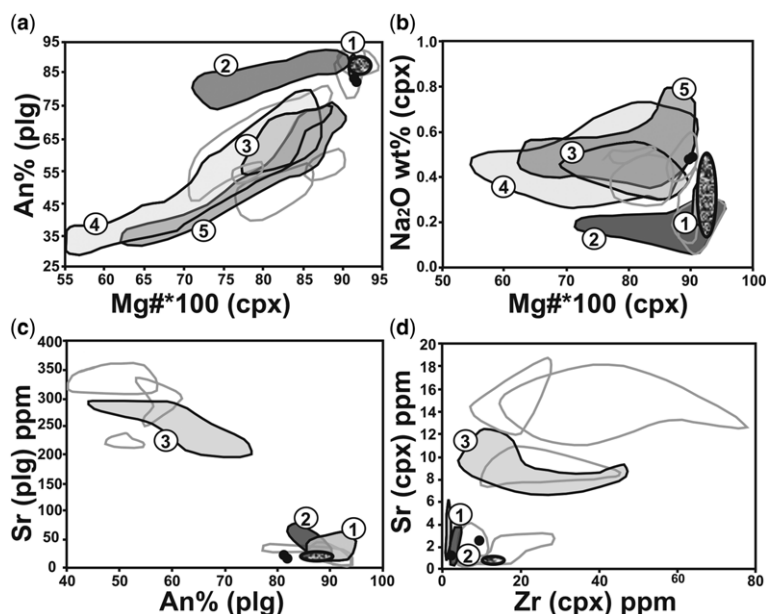


Fig. 9. Discriminant compositional parameters of minerals from the studied samples, plotted on diagrams of discriminant compositional parameters for clinopyroxenes and plagioclases of plagioclase-enriched peridotites and gabbro–norites from the Ligurian Tethys ophiolites (redrawn after Piccardo *et al.* 2014). Our investigated samples fall completely within the field of plagioclase-enriched peridotites and gabbro–norites, formed by strongly trace-element-depleted melts. Fields of analogous minerals from MORB olivine gabbros from the same ophiolite massifs are shown for comparison (redrawn and modified after Piccardo & Guarnieri 2011). Field 1: plagioclase-enriched peridotites (source of data: Rampone *et al.* 1997, 2005; Piccardo *et al.* 2007); field 2: gabbro–norites (source of data: Piccardo & Guarnieri 2011); field 3: MORB olivine gabbros from Erro–Tobbio (source of data: Borghini *et al.* 2007); field 4: MORB olivine gabbros from Internal Ligurides (source of data: Tribuzio *et al.* 1999); field 5: MORB olivine gabbros from Monte Maggiore (source of data: Piccardo & Guarnieri 2011). Note that gabbro–norites and plagioclase-enriched peridotites have: (i) cpx with high Mg#, very low Sr and Zr, and significantly low Na₂O; and (ii) plagioclases with unusually high An content and extremely low Sr content, with respect to the homologous minerals in n-MORB olivine gabbros, suggesting equilibration with primary, strongly trace-element-depleted melts.

rheological characteristics of the melt-interacted peridotites, causing their ‘rejuvenation’ (the trace-element and isotope equilibration with the percolating melts: i.e. the chemical erosion of the lithosphere) and the modification of their rheological characteristics (i.e. the thermo-mechanical erosion of the lithosphere) (see also the discussions in Piccardo 2014; Piccardo *et al.* 2014). These important modifications of the rheological characteristics of the lithosphere occurred up to shallow levels in the mantle lithosphere, until the heat loss by thermal conduction prevailed over heat supply by thermal advection of the percolating and crystallizing melts. This is clearly evidenced in ophiolites from fossil slow–ultraslow spreading basins (i.e. Ligurian Tethys, Othris) by the huge, mountain-size bodies of plagioclase-enriched peridotites, which are considered to represent: (1) refertilized mantle domains generated by melt stagnation in the shallow mantle lithosphere in embryonic oceans

and OCTs (Müntener *et al.* 2004, 2010; Piccardo *et al.* 2004a, b, c); and (2) melt stagnation and storage of strongly depleted melts in fossil and modern slow–ultraslow spreading oceans (Piccardo & Guarnieri 2011; Piccardo *et al.* 2014).

Conditions of thermal equilibration and thermal state of the lithosphere

Equilibration temperatures for the subsolidus recrystallization of the different metamorphic stages (spinel- to plagioclase- to amphibole-peridotite-facies recrystallization), recorded by the Erro–Tobbio peridotites and the shear zones unaffected by melt–peridotite reaction, have been obtained by Hoogerduijn Strating *et al.* (1993) and Rampone *et al.* (2005), applying various geothermometric methods based on major-element exchanges between coexisting mineral phases (i.e. Wells 1977; Sachtleben & Seck 1981; Brey & Köhler 1990;

Taylor 1998). These analyses yielded mean temperatures of 990–1090 °C for the oldest spinel-facies equilibration, and 960–970 °C for the subsequent spinel-facies tectonite recrystallization. Progressively decreasing temperatures are recorded by pyroxenes pertaining to the plagioclase- and amphibole-bearing peridotite granoblastic assemblages; these yielded average temperatures of 910–960 and 790–880 °C, respectively (data from Rampone *et al.* 2005).

The recognition of widespread diffuse melt percolation through the Erro–Tobbio peridotites (e.g. Piccardo 2003; Piccardo *et al.* 2004*b, c*; Rampone *et al.* 2005; Piccardo & Vissers 2007; and references therein), led Piccardo & Vissers (2007) to consider that diffuse porous flow of basaltic melts (at T of c. 1250 °C) in the originally rather cold (at T of c. 1000–1100 °C, according to the previous studies) Erro–Tobbio pristine mantle lithosphere requires that the thermal lithosphere was significantly heated by the rising asthenosphere and by melt percolation. This thermal effect should have caused the major- and trace-element equilibrium of all mineral phases at these high temperatures. However, systematic major-element variation between the core and rim of pyroxene porphyroclasts demonstrates that major-element homogenization was not achieved. For instance, the highest Al content is shown by the cores of pyroxene porphyroclasts, the lowest occur in the corresponding rims; Ca, Mg and Fe all show similar behaviour. In contrast, most trace elements in pyroxenes are remarkably homogeneous, independent of microstructural sites, indicating that near-complete trace-element equilibration was achieved during melt percolation, most probably in response to the high temperatures attained during melt percolation.

As discussed by Piccardo *et al.* (2007), the preservation of mostly equilibrated trace elements and variable major elements requires that trace-element distribution might be faster than major-element distribution. Experimental studies, as well as studies of natural rocks (Sneeringer *et al.* 1984; Griffin *et al.* 1996; Ionov *et al.* 2002; Van Orman *et al.* 2002), suggest that the diffusion velocity of many trace elements including REE in pyroxenes is significantly increased at increasing temperature, becoming higher than that of many major elements at about 1200 °C. The preservation of these characteristics also indicates that subsolidus re-equilibration under cooling during progressive exhumation was not able to significantly alter the mineral transition-element content. Thus, in order to discuss a consistent dataset of temperature estimates referable to the thermal peak conditions of the melt-percolation events, we calculated equilibration temperatures of the Erro–Tobbio melt-reacted spinel and plagioclase peridotites by

applying the empirical thermometers of Seitz *et al.* (1999), based on the partitioning of trace elements between coexisting opx and cpx. The Seitz *et al.* (1999) method has been tested on spinel-facies peridotites from the Malenco and Totalp subcontinental mantle rocks (i.e. Müntener & Hermann 1996; Manatschal & Nievergelt 1997), which have been interpreted as fragments of a former OCT. They yield T_{Sc} (T_{Sc} represents the temperature obtained using scandium) in the range 919–1046 °C, consistent with temperature estimates for the spinel-facies mantle lithosphere of the pre-extension system as follows.

Equilibration temperature estimates are calculated in each sample using core and rim compositions: the obtained temperature estimates do not change significantly, even in plagioclase-facies tectonites–mylonites where major-element core compositions (e.g. high Al content) most probably represent spinel-facies equilibration, whereas the major-element composition of rims, which are in textural equilibrium with plagioclase, represent plagioclase-facies equilibration. We obtain the following results:

- *melt-percolated protoliths*: T_{Sc} in the range 1207–1278 °C (calculated at $P = 20$ kbar) (average 1240 °C);
- *spinel-facies shear zones*: T_{Sc} in the range 1214–1234 °C (calculated at $P = 15$ kbar) (average 1220 °C);
- *plagioclase-facies shear zones*: T_{Sc} in the range 1209–1228 °C (calculated at $P = 5$ kbar) (average 1220 °C);
- *plagioclase peridotites*: T_{Sc} in the range 1123–1185 °C (calculated at $P = 5$ kbar; data from Romairone 1999) (average 1150 °C).

Closely similar results have been obtained by applying the empirical thermometer of Witt-Eickchen & O'Neill (2005), similarly based on the partitioning of trace elements between coexisting orthopyroxene and clinopyroxene. Applying the same Seitz *et al.* (1999) method, similar very high equilibration temperatures (in the range T_{Sc} 1200–1300 °C) have been obtained by Müntener & Piccardo (2003) for impregnated plagioclase peridotites from the Alps–Apennines ophiolitic peridotites and by Piccardo *et al.* (2007) for the South Lanzo melt-reacted peridotites (i.e. for reactive spinel peridotites, T_{Sc} frequently > 1220 °C; and for the plagioclase-enriched peridotites, T_{Sc} frequently c. 1200 °C). Note that high equilibrium temperatures for the South Lanzo plagioclase peridotites have also been reported by Pognante *et al.* (1985) and Bodinier *et al.* (1986).

The high equilibration T_{Sc} recorded by reactive spinel peridotites indicates that during the reactive melt infiltration the peridotites reached

temperatures close to the anhydrous peridotite solidus at spinel-facies pressure conditions. Analogously, the high T_{Sc} recorded by the plagioclase peridotites confirm that the melt interstitial crystallization occurred at high T_{Sc} under plagioclase-facies pressure conditions. Based on these data, it can be evidenced that very high temperatures, close to the dry peridotite solidus, were attained by the mantle lithosphere during percolation and impregnation by upwelling asthenospheric melts up to shallow lithospheric levels.

These data evidence that melt percolation though the extending lithosphere caused a significant heating (from *c.* 1000 to *c.* 1200 °C) close to asthenospheric conditions (i.e. asthenospherization) up to shallow lithospheric levels, suggesting significant melt thermal advection. It must be recalled that, in addition, thinning of the lithosphere would have been just as effective in raising temperatures, particularly where slow–ultraslow spreading was involved as there is time for heat advection to take place. This effect, which may be relevant during early melt-free extension, may become less important, however, when the extending lithospheric mantle undergoes rapid heating by porous melt-flow percolation and thermal advection.

We think that melt percolation and thermal advection, evidenced by the whole melt-reacted peridotites (i.e. reactive spinel harzburgites and plagioclase-enriched peridotites) of ophiolites from fossil slow–ultraslow spreading oceans (Ligurian Tethys, Othris), cannot be disregarded when presenting and discussing models for formation of OCT zones of slow spreading ridges. However, recent reviews of the tectonic, magmatic and hydrothermal evolution of slow spreading ridges that ‘emphasize the role of the thermal regime, as a key parameter for tectonic, magmatic and hydrothermal processes associated with continental breakup’ (Cannat *et al.* 2009, p. 16) do not properly take these mantle processes into account. Melt percolation, thermal advection, lithosphere thermal erosion and asthenospherization of the mantle lithosphere (i.e. Bodinier & Godard 2003; Piccardo 2003; Müntener *et al.* 2005), which characterize the rifting stages of slow–ultraslow spreading oceans (see the discussion in Piccardo *et al.* 2014 and references therein), cause dramatic modifications in the thermal (i.e. rheological) regime of the shallow mantle lithosphere along the axial zone of the extension system before drifting and seafloor spreading: that is, well before ‘the installation of a ridge-type thermal regime’ (Cannat *et al.* 2009, p. 1; Fig. 10).

A tentative and somewhat speculative pressure–temperature–time (P – T – t) diagram for the main steps of the evolution, which is also based on data and discussions in Piccardo (2014) and Piccardo *et al.* (2014), is presented in Figure 11.

Experimental constraints on lithosphere evolution during extension and rifting

The process by which tensional far-field stresses result in strain concentration and the formation of shear zones has been extensively studied (cf. for example Vissers *et al.* 1995; Regenauer-Lieb *et al.* 2006, 2008; Précigout & Gueydan 2009). The migration of mantle melts by either diffuse or channelled porous flow is estimated to range from a few metres to tens of metres per year (Ahern & Turcotte 1979; Kelemen *et al.* 1997; Ranalli *et al.* 2007; and references therein). The positive feedback between shear-zone formation and melt migration (e.g. see discussions by Brown & Solar 1998; Katz *et al.* 2006; Holtzman & Kohlstedt 2007; Muhlhaus *et al.* 2012) has important rheological consequences. The infiltration of melts initially at asthenospheric temperature results in considerable softening of the lithosphere (with a decrease in total strength from 10 to 1 N m⁻¹ as orders of magnitude: Ranalli *et al.* 2007), which in turn concentrates deformation in the infiltrated zone and is probably a factor in the continental extension–seafloor spreading transition, as envisaged by Piccardo (2003) and demonstrated by Ranalli *et al.* (2007) (see also the analogue models by Corti *et al.* 2007).

Increasingly powerful numerical models in two and three dimensions revealed the physical processes underlying extensional systems (Regenauer-Lieb *et al.* 2009 and references therein). They explored the sensitivity of extensional systems to the thermal structure of the lithosphere using numerical simulations applying thermodynamic-style models that use an energy feedback approach to derive spontaneous localization phenomena from the supposed underlying physical processes to geological problems. Regenauer-Lieb *et al.* (2009) show that the relatively new application of thermodynamic-style models (e.g. Regenauer-Lieb *et al.* 2001; Kaus & Podladchikov 2006; Braeck & Podladchikov 2007) provides evidence that the rheology of the lithosphere is controlled by weakening processes. Their numerical models show that during extension of an initially structurally uniform lithosphere, structures develop spontaneously out of basic thermodynamic energy fluxes. Regenauer-Lieb *et al.* (2009) remarked that the application of thermodynamic-style models has produced encouraging results such as the spontaneous development of a number of structures that match well-documented features of extensional systems, demonstrating that localization processes make the lithosphere weaker than previously estimated. These authors emphasize that: ‘in order to understand extensional systems it is necessary to take a multidisciplinary approach that integrates the dynamic evolution of lithospheric strength and

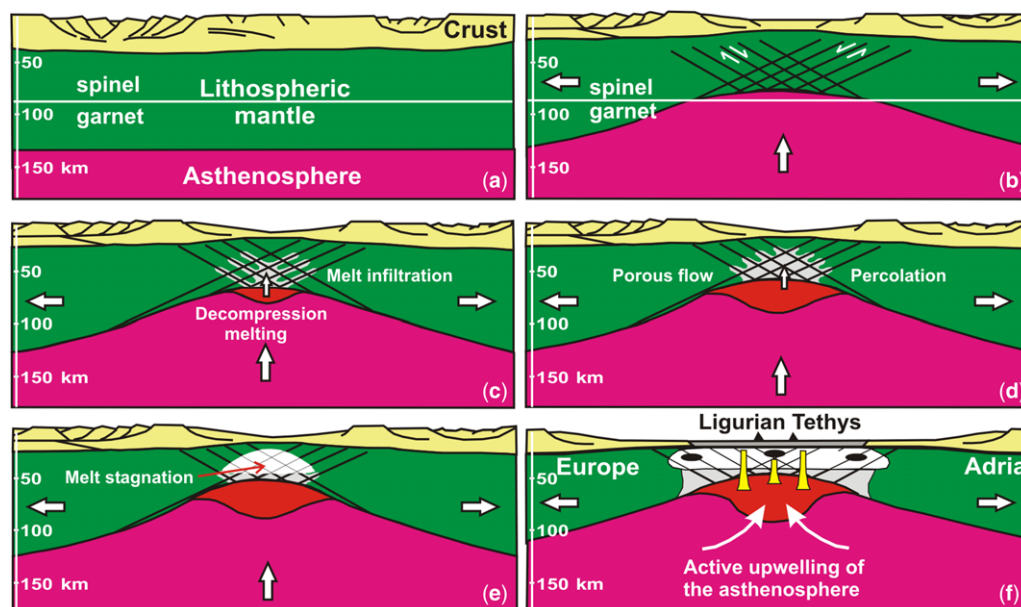


Fig. 10. Schematic diagrams describing the extensional evolution of the Ligurian Tethys, from pre-extension continental lithosphere to oceanic opening, based on present structural and petrological data, and, in particular, the interaction of tectonic and magmatic processes in the Ligurian Tethys from continental rifting to ocean formation (redrawn and modified after Piccardo *et al.* 2014). (a) Pre-extension (pre-Triassic?) setting. (b) Lithosphere extension by far-field tectonic forces that induce: (i) extensional shear-zone formation in the lithosphere; (ii) thinning of the lithosphere; and (iii) passive upwelling of the asthenosphere. (c) Onset of decompression melting in the passively upwelling asthenosphere. The passively upwelling asthenosphere may have reached melting conditions on decompression in a scattered way, and low-degree single-melt fractions were formed randomly under a regime of reduced melt production. This may have facilitated unmixing of single-melt increments in the asthenosphere. The produced single-melt increments infiltrated by diffuse porous and focused (i.e. along shear zones) flow through the lithosphere under spinel-facies conditions. Melt–peridotite reactions formed reactive spinel harzburgites. (d) Asthenosphere melting increased and the percolating melts transformed large sectors of the lower lithosphere to reactive peridotites. (e) Percolating melts became orthopyroxene(silica)-saturated by melt–rock reaction and reached shallower plagioclase-facies conditions where increasing heat loss by conduction led to melt stagnation and storage: melts impregnated peridotites as plagioclase-rich basaltic material and formed plagioclase-enriched peridotites and gabbro–norite pods. (f) Break-up of the crust and seafloor exposure of the melt-reacted and impregnated lithospheric peridotites. According to Piccardo *et al.* (2014), the weakened axial lithospheric wedge above the upwelling melting asthenosphere should have enhanced active upwelling of the deeper asthenosphere, thereby facilitating the transition from passive to active rifting and spreading. Intrusives and volcanics related to this stage indicate that asthenosphere melting formed aggregated MORB melts, suggesting that asthenosphere partial melting became more widespread, affected larger volumes, and that melt fractions were more efficiently mixed and homogenized (Piccardo *et al.* 2014). Spinel dunite channels were formed by infiltration and upwelling of strongly silica-depleted melts (MORBs?), under open-system conditions and at high melt/rock ratio, which dissolved all of the pyroxenes. These channels were exploited for upward migration of the aggregated MORB melts.

strain localization with a much deeper understanding of the multiple roles of mafic and felsic magmatism and the ability of the mantle to produce melt' (Regenauer-Lieb *et al.* 2008, p. 103).

We consider these results very important in understanding the localization of deformation, leading to physical anisotropy in the extending mantle lithosphere and formation of early shear zones in extensional systems. Recently, Muhlhaus *et al.* (2012) furnished an important contribution to understanding how melt flow is organized on lithospheric

scales. They modelled magma dynamics and tectonic processes, such as rifting, on the basis of equations governing the mechanical behaviour of a solid, deforming viscously in a pressure and temperature regime, and applying expressions for the shear viscosity proposed by Kelemen *et al.* (1997) and Zimmerman & Kohlstedt (2004). Their numerical analyses confirm the orientations of the localizations predicted in the linear instability analysis, whereby the localization increases with increasing power-law coefficient of the strain-rate-dependent

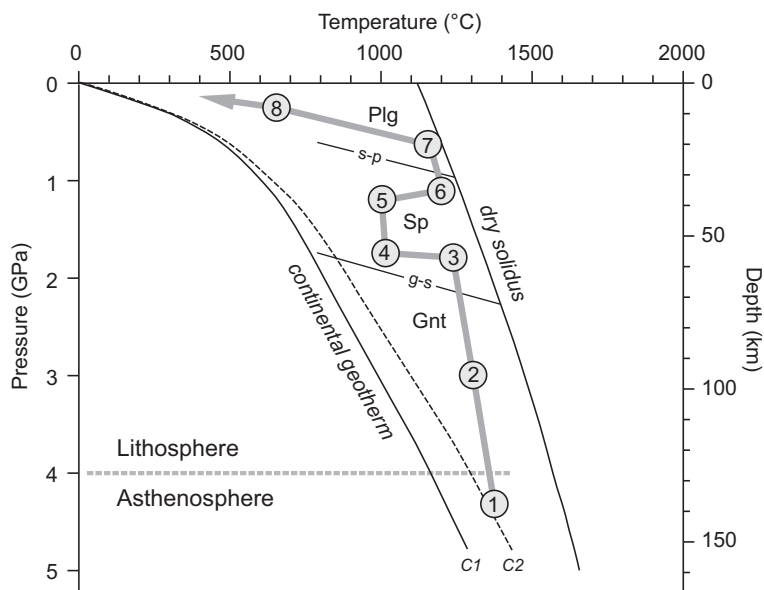


Fig. 11. Simplified P – T – t diagram showing the main stages in the evolution of the Erro–Tobbio peridotites as perceived in this study. Continental geotherms adopted from Jaupart & Mareschal (2007), calculated for a surface heat flux of 90 mW m^{-2} , and a Moho heat flux of 15 mW m^{-2} (C1) and 18 mW m^{-2} (C2). Dry peridotite solidus as proposed by Hirschmann (2000), based on post-1988 peridotite solidus data excluding enriched and depleted peridotite compositions. Lines s-p and g-s denote spinel-plagioclase- and garnet-spinel-facies boundaries; Plg, plagioclase facies; Sp, spinel facies; Gnt, garnet facies. The lithosphere–asthenosphere boundary (LAB) is shown at a maximum reference depth corresponding to 4.0 GPa. Note that the continental geotherms do not cross the dry peridotite solidus at that depth: the presence of fluids (e.g. melts, water) and increasing fluxing components (alkalis and FeO: i.e. increasing clinopyroxene content) in mantle peridotites at LAB could significantly depress the temperature conditions of the peridotite solidus towards the T values of the geothermal gradient at the reference pressure conditions. The main steps in the perceived P – T history are as follows: (1) residence in the asthenosphere (P and T highly speculative); (2) accretion to the lithosphere (P and T highly speculative), trajectory from (1) to (2) denotes asthenosphere accretion to the lithosphere under garnet-facies conditions (timing unknown); (3) spinel-facies conditions (P and T speculative), trajectory from (2) to (3) shows early exhumation from garnet- to spinel-facies conditions (timing unknown); (4) annealing recrystallization in the lithosphere towards a continental geotherm (P speculative, T of c. 1000°C , timing unknown); (5) almost adiabatic exhumation during early rifting stages (T average value 1000°C , onset of rifting probably Middle–Upper Permian); (6) increasing temperatures at decreasing pressures (exhumation, T of c. 1230°C), trajectory from (5) to (6) denotes thermal advection during exhumation due to porous melt-flow percolation under spinel-facies conditions, onset of reactive melt percolation Middle Jurassic; (7) plagioclase impregnation at high temperatures in plagioclase field (T average value 1180°C), trajectory from (6) to (7) reflects exhumation to plagioclase-facies conditions at high temperatures due to melt-assisted thermal advection (melt infiltration, reactive percolation and stagnation/crystallization), presumably during the Middle–Upper Jurassic; trajectory from (7) to (8) denotes progressive exhumation and cooling by conductive heat loss to shallow levels.

viscosity. Their analytical results indicate that high growth rates (and, hence, strong localization) are expected only for materials with strong strain dependence (high values of the strain-dependence exponent n). The strain concentration within the shear bands obtained for $n > 3$ is much more significant and consistent with results familiar from simulations based on plasticity models (Lemiale *et al.* 2008).

Muhlhaus *et al.* (2012, p. 2) showed that: ‘for a continental extension approach, melts are not even required at the initial rifting stages of continental

breakup’. For the formation of slow–ultraslow spreading oceans by slow–ultraslow continental extension, ‘this approach is more generally valid since it does not presuppose the existence of melts’.

Our structural and petrological data indicate that extension was melt-free at the onset (i.e. early spinel-facies shear zones are characterized by subsolidus syntectonic metamorphic features, whereas melt-related microstructural and compositional effects are completely lacking), and brought the deeper levels of the subcontinental lithosphere (garnet-facies peridotites) to shallower

spinel-peridotite-facies levels, before melts entered the system during ongoing extension. We recall that continental extension must have thinned the lithosphere by a factor 2 (i.e. to half of its original thickness) before the passively upwelling asthenosphere underwent partial melting under almost adiabatic decompression (Foucher *et al.* 1982; Corti *et al.* 2007; Ranalli *et al.* 2007; Piccardo *et al.* 2009).

To fully understand continental break-up and rifting processes, one would need to identify at what stage during continental extension melts do become an important factor. Muhlhaus *et al.* (2012) proposed a simple model to understand how melt flow is organized on lithospheric scales, which is an important goal in modelling magma dynamics and tectonic processes such as rifting. These authors confirmed a tendency for porosity and strain localizations to occur in extended lithosphere, the orientations of which were predicted in fully coupled, non-linear, finite-element simulations. They noted that: ‘the porosity in the localization bands is only about 30% higher than outside the bands for $n = 1$. The strain concentration within the shear bands obtained for $n > 3$ is much more significant and consistent with results familiar from simulations based on plasticity models (Lemiale *et al.* 2008)’ (Muhlhaus *et al.* 2012, p. 11). Since the presence of melt in the system represents an important weakening factor, it plays a central role in infiltration instabilities (Aharonov *et al.* 1995). The experimental evidence of porosity and strain localization in the extending lithosphere allows a better understanding of our field structures (i.e. the presence of melt-percolation channels within the extensional shear zones), which indicate that melt preferentially infiltrated along higher porosity bands (i.e. the porosity localization bands) inside the shear zones (i.e. the strain localization bands). Muhlhaus *et al.* (2012) emphasized that the application of these thermodynamic-style models requires further field-based testing and that, in order to understand extensional systems, it is necessary to take a multidisciplinary approach that integrates the dynamic evolution of lithospheric strength and strain localization with a much deeper understanding of the multiple roles of magmatism.

In this context, we believe that our field-based study yields an important dataset from a natural laboratory, as our structural and petrological investigations are based on mountain-wide, km-scale continuous outcrops of exposed mantle peridotites from the Alpine–Apennine orogenic belt. In summary, our data suggest that the subcontinental lithosphere was first thinned by the development of early extension-related shear zones, shear bands and porosity bands, which subsequently became infiltrated by reactive melts produced by the partial melting

of the underlying asthenosphere. These melts thus infiltrated along the previously melt-free shear and porosity bands, and percolated by diffuse porous flow through the host peridotite. As is well documented in fossil and modern slow–ultraslow spreading oceans, the inflow during the rifting stages of melts in the extensional system, percolating via porous flow through the extending lithosphere and stagnating at shallow lithospheric levels, is clearly responsible for thermal advection leading to ‘asthenospherization’. Melt ingress thus causes dramatic changes in the thermal regime of the extensional system, leading to further weakening and eventual break-up.

Concluding remarks

In this paper we investigated the structural, petrological and compositional features recorded by strongly deformed and melt-percolated Erro–Tobbio peridotites (Voltri Massif, Ligurian Alps, NW Italy), in order to demonstrate that the processes of shear-zone formation and melt percolation are linked by a positive feedback. Previous field and structural studies revealed that the mantle protolith has been deformed by up to km-scale shear zones that developed a tectonic–mylonitic foliation under spinel- and plagioclase-facies conditions in the absence of melts, and were solely percolated at very shallow levels by the downward infiltration of continental or oceanic hydrous fluids which formed hydrous (i.e. chlorite- and amphibole-bearing) syntectonic assemblages.

In this study, we have focused our field, structural and petrological–geochemical studies on spinel and plagioclase peridotites and extensional shear zones that underwent reactive percolation, both by porous and channelled upwelling of asthenospheric melts, in order to demonstrate that the processes of shear-zone formation and melt percolation are intimately linked. Our present results from the Erro–Tobbio peridotites lend strong support to powerful numerical models in two and three dimensions for the physical processes underlying extensional systems, and which demonstrate that, for continental extension and, in particular, for the formation of slow–ultraslow spreading oceans by slow–ultraslow continental extension, melts are not even required at the initial rifting stages, and also that extension leads to porosity and shear localization bands even in a previously unstructured lithosphere.

Our investigations thus allow a model for the inception of continental extension to rifting/drift of slow–ultraslow spreading oceans to be proposed, as evidenced by the field, structural and petrological–geochemical characteristics of the

Erro–Tobbio peridotites, in the context of lithospheric peridotites from the Ligurian Tethys ophiolites (see also Piccardo 2014; Piccardo *et al.* 2014):

- the subcontinental lithosphere was first extended and thinned by the development of shear zones, which could have developed from early-stage shear and porosity bands in the absence of melt in the system;
- the structured mantle peridotites were subsequently infiltrated by reactive melts, produced by the partial melting of the upwelling asthenosphere, both channelled along the previously melt-free structural/rheological bands, and percolating by diffuse porous flow through the host peridotite.

As is well documented in fossil and modern slow–ultraslow spreading oceans, this ingress of melts in the extensional system during the rifting stages may be responsible for thermal advection, leading to thermal erosion of the shallow mantle lithosphere and a consequent dramatic change in the dynamics of the system reflected in further weakening and eventual break-up. In fact, as emphasized by Piccardo *et al.* (2014), thermal advection along the axial zone of the extending lithosphere, above the asthenosphere melting zone, strongly modified the compositional and rheological characteristics of the percolated mantle lithosphere, forming a wedge-shaped softened and weakened zone between the future continental margins. Thus, the hotter/deeper asthenosphere found a preferential way for its active upwelling, causing a transition from passive rifting to active rifting.

Financial support was provided by the Italian MIUR (Ministero dell'Istruzione dell'Università e della Ricerca) to Giovanni B. Piccardo – Project PRIN2009 (mantle processes and tectonic–magmatic evolution at extensional settings). Matteo Padovano is grateful to the Italian MIUR for financially supporting his one-year scientific fellowship, dedicated to the main topic of this paper. Two anonymous reviewers are thanked for their comments on the manuscript. George Gibson managed the paper as volume editor.

References

- AHARONOV, E., WHITEHEAD, J. A., KELEMEN, P. B. & SPIEGELMAN, M. 1995. Channeling instability of upwelling melt in the mantle. *Journal of Geophysical Research*, **100**, 20 433–20 450.
- AHERN, J. L. & TURCOTTE, D. L. 1979. Magma migration beneath an ocean ridge. *Earth and Planetary Science Letters*, **45**, 115–122.
- BODINIER, J. L. & GODARD, M. 2003. Orogenic, ophiolitic, and abyssal peridotites. In: CARLSON, R. W. (ed.) *Geochemistry of the Mantle and Core*. Treatise on Geochemistry, **2**. Elsevier, Amsterdam, 103–170.
- BODINIER, J. L., GUIRAUD, M., DUPUY, C. & DOSTAL, J. 1986. Geochemistry of basic dikes in the Lanzo massif (Western Alps): petrogenetic and geodynamic implications. *Tectonophysics*, **128**, 77–95.
- BORGHINI, G., RAMPONE, E., CRISPINI, L., DE FERRARI, R. & GODARD, M. 2007. Origin and emplacement of ultramafic–mafic intrusions in the Erro–Tobbio mantle peridotite (Ligurian Alps, Italy). *Lithos*, **94**, 210–229.
- BOUDIER, F. 1978. Structure and petrology of the Lanzo peridotite massif (Piedmont Alps). *Geological Society of America Bulletin*, **89**, 1574–1591.
- BOUDIER, F. & NICOLAS, A. 1972. Fusion partielle gabbroïque dans la lherzolite de Lanzo (Alpes piémontaises). *Schweizerische Mineralogische und Petrographische Mitteilungen*, **52**, 39–56.
- BRAECK, S. & PODLADCHIKOV, Y. Y. 2007. Spontaneous thermal runaway as ultimate failure mechanism of materials. *Physical Review Letters*, **98**, 095504.
- BREY, G. P. & KÖHLER, T. 1990. Geothermobarometry in Four-phase lherzolites II. New thermobarometers, and practical assessment of existing thermobarometers. *Journal of Petrology*, **31**, 1353–1378.
- BROWN, M. & SOLAR, G. S. 1998. Shear-zone systems a 817 nd melts: feedback relations and self organization in orogenic belts. *Journal of Structural Geology*, **20**, 211–227.
- CANN, J. R., ELDERFIELD, H. & LAUGHTON, A. 1999. *Mid-Ocean Ridges. Dynamics of Processes Associated with Creation of New Oceanic Crust*. Cambridge University Press, Cambridge.
- CANNAT, M. 1996. How thick is the magmatic crust at slow spreading oceanic ridges? *Journal of Geophysical Research*, **101**, 2847–2857.
- CANNAT, M., CHATIN, F., WHITECHURCH, H. & CEULENEER, G. 1997. Gabbroic rocks trapped in the upper mantle at the Mid-Atlantic Ridge. In: KARSON, J. A., CANNAT, M., MILLER, D. J. & ELTHON, D. (eds) *Proceedings of the Ocean Drilling Program, Scientific Results*. Ocean Drilling Program, College Station, TX, **153**, 243–264.
- CANNAT, M., MANATSCHAL, G., SAUTER, D. & PERON-PINVIDIC, G. 2009. Assessing the conditions of continental breakup at magma-poor rifted margins: what can we learn from slow spreading mid-ocean ridges? *Comptes Rendus Geoscience*, **341**, 406–427.
- CAPITANIO, F. A. & GOES, S. 2006. Mesozoic spreading kinematics: consequences for Cenozoic Central and Western Mediterranean subduction. *Geophysical Journal International*, **165**, 804–816.
- CHIESA, S., CORTESOGNO, L. *ET AL.* 1975. Assetto strutturale ed interpretazione geodinamica del Gruppo di Voltri. *Bollettino della Società Geologica Italiana*, **94**, 555–581.
- CORTI, G., BONINI, M., INNOCENTI, F., MANETTI, P., PICCARDO, G. B. & RANALLI, G. 2007. Experimental models of extension of continental lithosphere weakened by percolation of asthenospheric melts. *Journal of Geodynamics*, **43**, 465–483.
- DICK, H. J. B. 1989. Abyssal peridotites, very slow spreading ridges and ocean ridge magmatism. In: SAUNDERS, A. D. & NORRY, M. J. (eds) *Magmatism in the Ocean Basins*. Geological Society, London, Special Publications, **42**, 71–105.

- DICK, H. J. B. & BULLEN, T. 1984. Chromian spinel as a petrogenetic indicator in abyssal and alpine-type peridotites and spatially associated lavas. *Contributions to Mineralogy and Petrology*, **86**, 54–76.
- DIJKSTRA, A. H., BARTH, M. G., DRURY, M. R., MASON, P. R. D. & VISSERS, R. L. M. 2003. Diffuse porous melt flow and melt-rock reaction in the mantle lithosphere at a slow spreading ridge: A structural petrology and LA-ICP-MS study of the Othris Peridotite Massif (Greece). *Geochemistry, Geophysics, Geosystems*, **4**, 8613, <http://dx.doi.org/10.1029/2001GC000278>
- DRURY, M. R., HOOGERDIJN STRATING, E. H. & VISSERS, R. L. M. 1990. Shear zone structures and microstructures in mantle peridotites from the Voltri massif, Ligurian Alps, N.W. Italy. *Geologie en Mijnbouw*, **69**, 3–17.
- FOUCHER, J. P., LE PICHON, X. *ET AL.* 1982. The ocean-continent transition in the uniform lithospheric stretching model: role of partial melting in the mantle [and discussion]. *Philosophical Transactions of the Royal Society A*, **305**, 27–43.
- FRISCH, W. 1979. Tectonic progradation and plate tectonic evolution of the Alps. *Tectonophysics*, **60**, 121–139.
- GRIFFIN, W. L., SMITH, D., RYAN, C. G., O'REILLY, S. Y. & WIN, T. T. 1996. Trace-element zoning in the mantle minerals: metasomatism and thermal events in the upper mantle. *The Canadian Mineralogist*, **34**, 1179–1193.
- GUARNIERI, L., NAKAMURA, E. *ET AL.* 2012. Petrology, trace element and SR, Nd, Hf isotope geochemistry of the North Lanzo peridotite massif (Western Alps, Italy). *Journal of Petrology*, **53**, 2259–2306.
- HART, S. R. & DUNN, T. 1993. Experimental cpx/melt partitioning of 24 trace elements. *Contributions to Mineralogy and Petrology*, **113**, 1–8.
- HELLEBRAND, E., SNOW, J. E., HOPPE, P. & HOFMANN, A. W. 2002. Garnet field melting and late-stage refertilization in 'residual' abyssal peridotites from the Central Indian Ridge. *Journal of Petrology*, **43**, 2305–2338.
- HIRSCHMANN, M. M. 2000. Mantle solidus: experimental constraints and the effects of peridotite composition. *Geochemistry, Geophysics, Geosystems*, **1**, 2000GC000070.
- HOFMANN, A. W. 1988. Chemical differentiation of the earth: the relationship between mantle, continental crust and oceanic crust. *Earth and Planetary Science Letters*, **90**, 297–314.
- HOLTZMAN, B. & KOHLSTEDT, D. L. 2007. Stress-driven melt segregation and strain partitioning in partially molten rocks: effects of stress and strain. *Journal of Petrology*, **48**, 2379–2406.
- HOOGERDIJN STRATING, E. H., PICCARDO, G. B., RAMPONE, E., SCAMBELLURI, M. & VISSERS, R. L. M. 1990. The structure of the Erro–Tobbio peridotite (Voltri Massif, Ligurian Alps); a two day excursion with emphasis on processes in the upper mantle. *Ophioliti*, **15**, 119–184.
- HOOGERDIJN STRATING, E. H., RAMPONE, E., PICCARDO, G. B., DRURY, M. & VISSERS, R. L. M. 1993. Subsolidus emplacement of mantle peridotites during incipient oceanic rifting and opening of the Mesozoic Tethys (Voltri Massif, NW Italy). *Journal of Petrology*, **34**, 901–927.
- IONOV, D. A., BODINIER, J. L., MUKASA, S. B. & ZANETTI, A. 2002. Mechanisms and sources of mantle metasomatism: major and trace element conditions of peridotite xenoliths from Spitzbergen in the context of numerical modelling. *Journal of Petrology*, **43**, 2219–2259.
- JAUPART, C. & MARESCHAL, J.-C. 2007. Heat flow and thermal structure of the lithosphere. In: WATTS, A. B. (ed.) *Crust and Lithosphere Dynamics. Treatise on Geophysics*, **6**. Elsevier, Amsterdam, 217–251.
- JOHNSON, K. T. M., DICK, H. J. B. & SHIMIZU, N. 1990. Melting in the oceanic upper mantle: an ion microprobe study of diopsides in abyssal peridotites. *Journal of Geophysical Research – Solid Earth and Planets*, **95**, 2661–2678.
- KATZ, R. F., SPIEGELMAN, M. & HOLTZMAN, B. 2006. The dynamics of melt and shear localization in partially molten aggregates. *Nature*, **442**, 676–679.
- KAUS, B. J. P. & PODLADCHIKOV, Y. Y. 2006. Initiation of localized shear zones in visco-elastoplastic rocks. *Journal of Geophysical Research*, **111**, B04412, <http://dx.doi.org/10.1029/2005JB003652>
- KELEMEN, P. B. 1990. Reaction between ultramafic rock and fractionating basaltic magma I. Phase relations, the origin of calc-alkaline magma series, and the formation of discordant dunite. *Journal of Petrology*, **31**, 51–98.
- KELEMEN, P. B., DICK, H. J. B. & QUICK, J. E. 1992. Formation of harzburgite by pervasive melt/rock reaction in the upper mantle. *Nature*, **358**, 635–641.
- KELEMEN, P. B., WHITEHEAD, J. A., AHARONOV, E. & JORDAHL, K. A. 1995. Experiments on flow focusing in soluble porous media, with applications to melt extraction from the mantle. *Journal of Geophysical Research*, **100**, 475–496.
- KELEMEN, P. B., HIRTH, G., SHIMIZU, N., SPIEGELMAN, M. & DICK, H. J. B. 1997. A review of melt migration processes in the adiabatically upwelling mantle beneath oceanic spreading ridges. *Philosophical Transactions of the Royal Society of London Series A: Mathematical, Physical and Engineering Sciences*, **355**, 283–318.
- LAGABRIELLE, Y. & CANNAT, M. 1990. Alpine Jurassic ophiolites resemble the modern central Atlantic basement. *Geology*, **18**, 319–322.
- LAGABRIELLE, Y. & LEMOINE, M. 1997. Alpine, Corsican and Apennine ophiolites: the slow spreading ridge model. *Comptes Rendus Geoscience*, **325**, 909–920.
- LEMIALE, V., MUHLHAUS, H. B., MORESI, L. & STAFFORD, J. 2008. Shear banding analysis of plastic models formulated for incompressible viscous flows. *Physics of the Earth and Planetary Interiors*, **171**, 177–186.
- LEMOINE, M., TRICART, P. & BOILLLOT, G. 1987. Ultramafic and gabbroic ocean floor of the Ligurian Tethys (Alps, Corsica, Apennines). In search of a genetic model. *Geology*, **15**, 622–625.
- LI, X. H., FAURE, M., LIN, W. & MANATSCHAL, G. 2013. New isotopic constraints on age and magma genesis of an embryonic oceanic crust: the Chenaillet Ophiolite in the Western Alps. *Lithos*, **160–161**, 283–291.
- MAGDE, L. S., BARCLAY, A. H., TOOMEY, D. R., DETRICK, R. S. & COLLINS, J. A. 2000. Crustal magma plumbing within a segment of the Mid-Atlantic Ridge, 35°N. *Earth and Planetary Science Letters*, **175**, 55–67.

- MALATESTA, C., CRISPINI, L., FEDERICO, L., CAPPONI, G. & SCAMBELLURI, M. 2011. The exhumation of high pressure ophiolites (Voltri Massif, Western Alps): insights from structural and petrologic data on meta-gabbro bodies. *Tectonophysics*, **568–569**, 102–123.
- MALATESTA, C., CRISPINI, L., FEDERICO, L., CAPPONI, G. & SCAMBELLURI, M. 2012a. The exhumation of high pressure ophiolites (Voltri Massif, Western Alps): insights from structural and petrologic data on meta-gabbro bodies. *Tectonophysics*, **568–569**, 102–123.
- MALATESTA, C., GERYA, T., SCAMBELLURI, M., FEDERICO, L. & CRISPINI, L. 2012b. Intraoceanic subduction of 'heterogeneous' oceanic lithosphere in narrow basins: 2D numerical modeling. *Lithos*, **140–141**, 234–251.
- MANATSCHAL, G. & NIEVERGELT, P. 1997. A continent–ocean transition recorded in the Err and Platta nappes (Eastern Switzerland). *Eclogae Geologicae Helveticae*, **90**, 3–27.
- MESSIGA, B. & PICCARDO, G. B. 1974. Rilevamento geotografico e strutturale del Gruppo di Voltri. Il settore nord-orientale: la zona fra M. Tacco e M. Orditano. *Memorie della Società Geologica Italiana*, **13**, 301–315.
- MONTANINI, A., TRIBUZIO, R. & ANCKIEWICZ, R. 2006. Exhumation history of a garnet pyroxenite bearing mantle section from a continent–ocean transition (Northern Apennine ophiolites, Italy). *Journal of Petrology*, **47**, 1943–1971.
- MUHLHAUS, H., MOHAJERI, A., FINZI, Y. & REGENAUER-LIEB, K. 2012. The orientation of melt bands in an extending lithosphere. In: EBERHARDSTEINER, J. (ed.) *6th European Congress on Computational Methods in Applied Sciences and Engineering (ECCOMAS 2012)*, September 10–14, 2012, Vienna, Austria. Vienna University of Technology, Vienna, 7344–7356.
- MÜNTENER, O. & HERMANN, J. 1996. The Val Malenco lower crust–upper mantle complex and its field relations (Italian Alps). *Schweizerische Mineralogische und Petrographische Mitteilungen*, **76**, 475–500.
- MÜNTENER, O. & HERMANN, J. 2001. The role of lower crust and continental upper mantle during formation of non-volcanic passive margins: Evidence from the Alps. In: WILSON, R. C. L., WHITMARSH, R. B., TAYLOR, B. & FROITZHEIM, N. (eds) *Non-volcanic Rifting of Continental Margins: A Comparison of Evidence from Land and Sea*. Geological Society, London, Special Publications, **187**, 267–288.
- MÜNTENER, O. & PICCARDO, G. B. 2003. Melt migration in ophiolites: the message from Alpine–Apennine peridotites and implications for embryonic ocean basins. In: DILEK, Y. & ROBINSON, P. T. (eds) *Ophiolites in Earth History*. Geological Society, London, Special Publications, **218**, 69–89.
- MÜNTENER, O., PETTKE, T., DESMURS, L., MEIER, M. & SCHALTEGGER, U. 2004. Refertilization of mantle peridotite in embryonic ocean basins: trace element and Nd isotopic evidence and implications for crust–mantle relationships. *Earth and Planetary Science Letters*, **221**, 293–308.
- MÜNTENER, O., PICCARDO, G. B., POLINO, R. & ZANETTI, A. 2005. Revisiting the Lanzo peridotite (NW-Italy): 'asthenospherization' of ancient mantle lithosphere. *Ophioliti*, **30**, 111–124.
- MÜNTENER, O., MANATSCHAL, G., DESMUR, L. & PETTKE, T. 2010. Plagioclase peridotites in ocean–continent transitions: refertilized mantle domains generated by melt stagnation in the shallow mantle lithosphere. *Journal of Petrology*, **51**, 255–294.
- PICCARDO, G. B. 2003. Mantle processes during ocean formation: petrologic records in peridotites from the Alpine–Apennine ophiolites. *Episodes*, **26**, 193–200.
- PICCARDO, G. B. 2008. The Jurassic Ligurian Tethys, a fossil ultraslow-spreading ocean: the mantle perspective. In: COLTORTI, M. & GRÉGOIRE, M. (eds) *Metasomatism in Oceanic and Continental Lithospheric Mantle*. Geological Society, London, Special Publications, **293**, 11–34.
- PICCARDO, G. B. 2010. The evolution of the lithospheric mantle during Mesozoic rifting in the Ligure–Piedmontese domain. In: BELTRANDO, M., PECCERILLO, A., MATTEI, M., CONTICELLI, S. & DOGLIONI, C. (eds) *The Geology of Italy: Tectonics and Life Along Plate Margins. Journal of the Virtual Explorer*, **36**, 7, <http://dx.doi.org/10.3809/jvirtex.2010.00219>
- PICCARDO, G. B. 2012. Subduction of a fossil slow–ultraslow spreading ocean: a petrology constrained geodynamic model based on the Voltri Massif, Ligurian Alps, Northwest Italy. *International Geology Review*, *iFirst*, **2012**, 1–17.
- PICCARDO, G. B. 2013. Reply to the comment by Marco Scambelluri on the paper: 'Subduction of a fossil slow-ultraslow spreading ocean: a petrology-constrained geodynamic model based on the Voltri Massif, Ligurian Alps, NW Italy' by G. B. Piccardo. *International Geology Review*, **55**, <http://dx.doi.org/10.1080/00206814.2013.782967>
- PICCARDO, G. B. 2014. Passive rifting and continental splitting in the Jurassic Ligurian Tethys: the mantle perspective. In: GIBSON, G. M., ROURE, F. & MANATSCHAL, G. (eds) *Sedimentary Basins and Crustal Processes at Continental Margins: From Modern Hyper-extended Margins to Deformed Ancient Analogues*. Geological Society, London, Special Publications, **413**. First published online November 10, 2014, <http://dx.doi.org/10.1144/SP413.4>
- PICCARDO, G. B. & GUARNIERI, L. 2011. Gabbro–norite cumulates from strongly depleted MORB melts in the Alpine–Apennine ophiolites. *Lithos*, **124**, 210–214.
- PICCARDO, G. B. & VISSERS, R. L. M. 2007. The pre-oceanic evolution of the Erro-Tobbio peridotite (Voltri Massif, Ligurian Alps, Italy). *Journal of Geodynamics*, **43**, 417–449.
- PICCARDO, G. B., CORTESOGNO, L., MESSIGA, B., GALLI, M. & PEDEMONTE, G. M. 1977. Excursion to the metamorphic ophiolites of the Gruppo di Voltri. *Rendiconti della Società Italiana di Mineralogia e Petrologia*, **33**, 295–314.
- PICCARDO, G. B., RAMPONE, E. & SCAMBELLURI, M. 1989. The alpine evolution of the Erro-Tobbio peridotites (Voltri Massif–Ligurian Alps): some field and petrographic constraints. *Ophioliti*, **13**, 169–174.
- PICCARDO, G. B., MÜNTENER, O. & ZANETTI, A. 2004a. Alpine–Apennine ophiolitic peridotites: new concepts on their composition and evolution. *Ophioliti*, **28**, 19–36.

- PICCARDO, G. B., MÜNTENER, O., ZANETTI, A. & PETTKE, T. 2004b. Ophiolitic peridotites of the Alpine–Apennine system: mantle processes and geodynamic relevance. *International Geology Review*, **46**, 1119–1159.
- PICCARDO, G. B., MÜNTENER, O., ZANETTI, A., ROMAIRONE, A., BRUZZONE, S., POGGI, E. & SPAGNOLO, G. 2004c. The Lanzo South peridotite: melt/peridotite interaction in the mantle lithosphere of the Jurassic Ligurian Tethys. *Ophioliti*, **29**, 37–62.
- PICCARDO, G. B., ZANETTI, A. & MÜNTENER, O. 2007. Melt/peridotite interaction in the Lanzo South peridotite: field, textural and geochemical evidence. *Lithos*, **94**, 181–209.
- PICCARDO, G. B., VANNUCCI, R. & GUARNIERI, L. 2009. Evolution of the lithospheric mantle in an extensional setting: insights from ophiolitic peridotites. *Lithosphere*, **1**, 81–87.
- PICCARDO, G. B., PADOVANO, M. & GUARNIERI, L. 2014. The Ligurian Tethys: mantle processes and geodynamics. *Earth-Science Reviews*, **138**, 409–434, <http://dx.doi.org/10.1016/j.earscirev.2014.07.002>
- POGNANTE, U., RÖSLI, U. & TOSCANI, L. 1985. Petrology of ultramafic and mafic rocks from the Lanzo peridotite body (Western Alps). *Lithos*, **18**, 201–214.
- PRÉCIGOUT, J. & GUEYDAN, F. 2009. Mantle weakening and strain localization: implications for the long-term strength of the continental lithosphere. *Geology*, **37**, 147–150.
- RABAIN, A., CANNAT, M., ESCARTIN, J., POULIQUEN, G., DEPLUS, C. & ROMMEVAUX JESTIN, G. 2001. Focused volcanism and growth of a slow spreading segment (Mid-Atlantic Ridge, 35°N). *Earth and Planetary Science Letters*, **185**, 211–224.
- RAMPONE, E. & PICCARDO, G. B. 2000. The ophiolite–oceanic lithosphere analogue: new insights from the Northern Apennines (Italy). In: DILEK, Y., MOORES, E. M., ELTHON, D. & NICOLAS, A. (eds) *Ophiolites and Oceanic Crust: New Insights from Field Studies and the Oceanic Drilling Program*. Geological Society of America, Special Papers, **349**, 21–34.
- RAMPONE, E., PICCARDO, G. B., VANNUCCI, R. & BOTTAZZI, P. 1997. Chemistry and origin of melts in ophiolitic peridotites. *Geochimica et Cosmochimica Acta*, **61**, 4557–4569.
- RAMPONE, E., ROMAIRONE, A. & HOFMANN, A. W. 2004. Contrasting bulk and mineral chemistry in depleted peridotites: evidence for reactive porous flow. *Earth and Planetary Science Letters*, **218**, 491–506.
- RAMPONE, E., ROMAIRONE, A., ABOUCHAMI, W., PICCARDO, G. B. & HOFMANN, A. W. 2005. Chronology, petrology and isotope geochemistry of the Erro–Tobbio peridotites (Ligurian Alps, Italy): records of Late Palaeozoic lithospheric extension. *Journal of Petrology*, **46**, 799–827.
- RAMPONE, E., HOFMANN, A. W. & RACZEK, I. 2009. Isotopic equilibrium between mantle peridotite and melt: evidence from the Corsica ophiolite. *Earth and Planetary Science Letters*, **15**, 601–610.
- RANALLI, G., PICCARDO, G. B. & CORONA-CHAVEZ, P. 2007. Softening of the subcontinental lithospheric mantle by asthenosphere melts and the continental extension/oceanic spreading transition. *Journal of Geodynamics*, **43**, 450–464.
- REGENAUER-LIEB, K., YUEN, D. A. & BRANLUND, J. 2001. The initiation of subduction: criticality by addition of water? *Science*, **294**, 278–280.
- REGENAUER-LIEB, K., WEINBERG, R. F. & ROSENBAUM, G. 2006. The effect of energy feedbacks on continental strength. *Nature*, **442**, 67–70.
- REGENAUER-LIEB, K., ROSENBAUM, G. & WEINBERG, R. F. 2008. Strain localisation and weakening of the lithosphere during extension. *Tectonophysics*, **458**, 96–104.
- REGENAUER-LIEB, K., HOBBS, B., ORD, A., OLIVER, G. & VERNON, R. 2009. Deformation with coupled chemical diffusion. *Physics of the Earth and Planetary Interiors*, **172**, 43–54.
- ROMAIRONE, A. 1999. *Petrologia, Geochimica e Geochimica Isotopica delle peridotiti dell'Unità Erro-Tobbio (Gruppo di Voltri)*. PhD thesis, University of Genova.
- SACHTLEBEN, TH. & SECK, H. A. 1981. Chemical control of Al-solubility in orthopyroxene and its implications on pyroxene geothermometry. *Contributions to Mineralogy and Petrology*, **78**, 157–165.
- SCAMBELLURI, M., HOOGERDUIN STRATING, E. H., PICCARDO, G. B., VISSERS, R. L. M. & RAMPONE, E. 1991. Alpine olivine and titanite clinohumite bearing assemblages in the Erro–Tobbio peridotites. *Journal of Metamorphic Geology*, **9**, 79–91.
- SCHMID, S. M., FÜGENSCHUH, B., KISSLING, E. & SCHUSTER, R. 2004. Tectonic map and overall architecture of the Alpine orogen. *Ecolae Geologicae Helvetiae*, **97**, 93–117.
- SEITZ, H. M., ALTHERR, R. & LUDWIG, T. 1999. Partitioning of transition elements between orthopyroxene and clinopyroxene in peridotitic and websteritic xenoliths: new empirical geothermometers. *Geochimica et Cosmochimica Acta*, **63**, 3967–3982.
- SNEERINGER, M., HART, S. R. & SHIMIZU, N. 1984. Strontium and samarium diffusion in diopside. *Geochimica et Cosmochimica Acta*, **48**, 1589–1608.
- TAYLOR, W. R. 1998. An experimental test of some geothermometer and geobarometer formulations for upper mantle peridotites with application to the thermobarometry of fertile lherzolite and garnet websterite. *Neues Jahrbuch für Mineralogie, Abhandlungen*, **172**, 381–408.
- TIEPOLO, M., OBERTI, R. & VANNUCCI, R. 2002. Trace-element incorporation in titanite: constraints from experimentally determined solid/liquid partition coefficients. *Chemical Geology*, **191**, 105–119.
- TRIBUZIO, R., TIEPOLO, M., VANNUCCI, R. & BOTTAZZI, P. 1999. Trace element distribution within the olivine-bearing gabbros from the Northern Apennine ophiolites (Italy): evidence for post-cumulus crystallization in MOR-type gabbroic rocks. *Contributions to Mineralogy and Petrology*, **134**, 123–133.
- TRIBUZIO, R., THIRLWALL, M. F. & VANNUCCI, R. 2000. Evolution of gabbroic rocks of the Northern Apennine ophiolites (Italy): comparison with the lower oceanic crust from modern slow spreading ridges. In: DILEK, Y., MOORES, E. M., ELTHON, D. & NICOLAS, A. (eds) *Ophiolites and Oceanic Crust: New Insights from Field Studies and the Oceanic Drilling Program*. Geological Society of America, Special Papers, **349**, 129–138.

- VAN ORMAN, J. A., GROVE, T. L. & SHIMIZU, N. 2002. Diffusive fractionation of trace elements during production and transport of melt in Earth's upper mantle. *Earth and Planetary Science Letters*, **198**, 93–112.
- VERNIÈRES, L., GODARD, M. & BODINIER, J. L. 1997. A plate model for the simulation of trace element fractionation during partial melting and magma transport in the Earth's upper mantle. *Journal of Geophysical Research*, **102**, 24 771–24 784.
- VISSERS, R. L. M., DRURY, M. R., HOOGERDIJN-STRATING, E. H. & VAN DER WAL, D. 1991. Shear zones in the upper mantle: a case study in an Alpine lherzolite massif. *Geology*, **19**, 990–993.
- VISSERS, R. L. M., DRURY, M. R., HOOGERDIJN-STRATING, E. H., SPIERS, C. J. & VAN DER WAL, D. 1995. Mantle shear zones and their effect on lithosphere strength during continental breakup. *Tectonophysics*, **249**, 155–171.
- VISSERS, R. L. M., VAN HINSBERGEN, D. J. J., MEIJER, P. Th. & PICCARDO, G. B. 2013. Kinematics of Jurassic ultra-slow spreading in the Piemonte Ligurian ocean. *Earth and Planetary Science Letters*, **380**, 138–150.
- WELLS, P. R. A. 1977. Pyroxene thermometry in simple and complex systems. *Contributions to Mineralogy and Petrology*, **62**, 129–139.
- WHITMARSH, R. B. & MANATSCHAL, G. 2012. Evolution of magma poor continental margins: from rifting to the onset of seafloor spreading. In: ROBERTS, B. G. & BALLY, A. W. (eds) *Regional Geology and Tectonics: Phanerozoic Passive Margins, Cratonic Basins and Global Tectonic Maps*, Volume **1C**. Elsevier, Amsterdam, 326–341, <http://dx.doi.org/10.1016/B978-0-444-56357-6.00008-1>
- WITT-EICKSCHEN, G. & O'NEILL, H. St. C. 2005. The effect of temperature on the equilibrium distribution of trace elements between clinopyroxene, orthopyroxene, olivine and spinel in upper mantle peridotite. *Chemical Geology*, **221**, 65–101.
- ZIMMERMAN, M. E. & KOHLSTEDT, D. L. 2004. Rheological properties of partially molten lherzolite. *Journal of Petrology*, **45**, 275–298.